J Neuropathol Exp Neurol
Vol. 81, No. 9, September 2022, pp. 666–695
doi: 10.1093/jnen/nlac056

OXFORD

ORIGINAL ARTICLE

SARS-CoV-2 Brain Regional Detection, Histopathology, Gene Expression, and Immunomodulatory Changes in Decedents with COVID-19

Geidy E. Serrano, PhD, Jessica E. Walker, BS, Cécilia Tremblay, PhD, Ignazio S. Piras, PhD, Matthew J. Huentelman, PhD, Christine M. Belden, PsyD, Danielle Goldfarb, MD, David Shprecher, MD, Alireza Atri, MD, PhD, Charles H. Adler, MD, PhD, Holly A. Shill, MD, Erika Driver-Dunckley, MD, Shyamal H. Mehta, MD, Richard Caselli, MD, Bryan K. Woodruff, MD, Chadwick F. Haarer, MD, Thomas Ruhlen, MD, Maria Torres, MD, Steve Nguyen, MD, Dasan Schmitt, MD, Steven Z. Rapscak, MD, Christian Bime, MD, Joseph L. Peters, MD, Ellie Alevritis, MD, Richard A. Arce, BS, Michael J. Glass, BS, Daisy Vargas, BS, Lucia I. Sue, BS, Anthony J. Intorcia, BS, Courtney M. Nelson, BS, Javon Oliver, BS, Aryck Russell, BS, Katsuko E. Suszczewicz, BS, Claryssa I. Borja, BS, Madison P. Cline, MS, Spencer J. Hemmingsen, MS, Sanaria Qiji, BS, Holly M. Hobgood, BS, Joseph P. Mizgerd, PhD, Malaya K. Sahoo, PhD, Haiyu Zhang, PhD, Daniel Solis, BS, Thomas J. Montine, MD, PhD, Gerald J. Berry, MD, Eric M. Reiman, MD, PhD, Katharina Röltgen, PhD, Scott D. Boyd, MD, PhD, Benjamin A. Pinsky, MD, PhD, James L. Zehnder, MD, PhD, Pierre Talbot, PhD, Marc Desforges, PhD, Michael DeTure, PhD, Dennis W. Dickson, MD, and Thomas G. Beach, MD, PhD

From the Banner Sun Health Research Institute, Sun City, Arizona, USA (GES, JEW, CT, CMB, DG, DS, AA, RAA, MJG, DV, LIS, AJI, CMN, JO, KES, CIB, MPC, SJH, SQ, HMH, TGB); Neurogenomics Division, Translational Genomics Research Institute, Phoenix, Arizona, USA (ISP, MJH); Brigham and Women's Hospital and Harvard Medical School, Boston, Massachusetts, USA (AA); Mayo Clinic College of Medicine, Mayo Clinic Arizona, Scottsdale, Arizona, USA (CHA, EDD, SHM, RC, BKW); Barrow Neurological Institute, Phoenix, Arizona, USA (HAS); Banner Boswell Medical Center, Sun City, Arizona, USA (CFH, TR, MT, SN, DS, JLP, EA); Banner Alzheimer's Institute, Tucson, Arizona, USA (SZR); Banner University Medical Center, Tucson, Arizona, USA (CB); Uniformed Services University of the Health Sciences, Bethesda, Maryland, USA (AR); Pulmonary Center, Boston University School of Medicine, Boston, Massachusetts, USA (JPM); Department of Pathology, Stanford University, Stanford, California, USA (MKS, HZ, DS, TJM, GJB, KR, SDB, BAP, JLZ); Banner Alzheimer's Institute, Phoenix, Arizona, USA (EMR); Division of Infectious Disease & Geographic Medicine, Department of Medicine, Stanford University, Stanford, California, USA (BAP); Laboratory of Neuroimmunology, Centre Armand-Frappier Santé Biotechnologie, Institut National de la Recherche Scientifique, Laval, Quebec, Canada (PT); Laboratory of Virology, Centre Hospitalier Universitaire Sainte-Justine, Montréal, Quebec, Canada (MD); Département de microbiologie, infectiologie et Immunologie, Université de Montréal, Montréal, Quebec, Canada (MD); Mayo Clinic College of Medicine, Mayo Clinic Florida, Jacksonville, Florida, USA (MD, DWD).

Send correspondence to: Thomas G. Beach, MD, PhD, Banner Sun Health Research Institute, 10515 West Santa Fe Drive, Sun City, AZ 85351, USA; E-mail: thomas.beach@bannerhealth.com.

Geidy E. Serrano and Thomas G. Beach contributed equally to this work.

This project was supported by a COVID-19 Supplement to a National Institute on Aging grant (3P30AG019610-20S1), submitted in response to a Notice of Special Interest (NOSI) issued by the National Institute on Aging (NOT-AG-20-022). Other support was provided by National Institute on Aging grants P30AG19610 and P30AG072980 to the Arizona Alzheimer's Disease Research Center.

The authors have no duality or conflicts of interest to declare.

Supplementary Data can be found at academic.oup.com/jnen.

Abstract

Brains of 42 COVID-19 decedents and 107 non-COVID-19 controls were studied. RT-PCR screening of 16 regions from 20 COVID-19 autopsies found SARS-CoV-2 E gene viral sequences in 7 regions (2.5% of 320 samples), concentrated in 4/20 subjects (20%). Additional screening of olfactory bulb (OB), amygdala (AMY) and entorhinal area for E, N1, N2, RNA-dependent RNA polymerase, and S gene sequences detected one or more of these in OB in 8/21 subjects (38%). It is uncertain whether these RNA sequences represent viable virus. Significant histopathology was limited to 2/42 cases (4.8%), one with a large acute cerebral infarct and one with hemorrhagic encephalitis. Case-control RNAseq in OB and AMY found more than 5000 and 700 differentially expressed genes, respectively, unrelated to RT-PCR results; these involved immune response, neuronal constituents, and olfactory/taste receptor genes. Olfactory marker protein-1 reduction indicated COVID-19-related loss of OB olfactory mucosa afferents. Iba-1-immunoreactive microglia had reduced area fractions in cerebellar cortex and AMY, and cytokine arrays showed generalized downregulation in AMY and upregulation in blood serum in COVID-19 cases. Although OB is a major brain portal for SARS-CoV-2, COVID-19 brain changes are more likely due to blood-borne immune mediators and trans-synaptic gene expression changes arising from OB deafferentation.

Key Words: Amygdala, Cytokine, Deafferentation, Encephalitis, Microglia, Olfactory bulb, SARS-Cov-2.

INTRODUCTION

The coronavirus SARS-CoV-2 is primarily associated with severe respiratory disease, termed COVID-19, but there have been numerous reports of an accompanying broad range of neurological signs, symptoms, and syndromes, affecting up to 36% of patients (1–10). The causes are unclear, as multiple published studies and reviews (11–40) generally agree, with a few exceptions, that substantial SARS-CoV-2 brain invasion occurs in only a minority of fatal COVID-19 cases.

Although isolated case reports of meningitis and/or encephalitis exist (27, 33, 34, 41–45), and despite variation in findings, there is also general agreement that specific histopathological features are most often lacking in postmortem COVID-19 brains (12–16, 18, 19, 25, 26, 28, 29, 32–34, 36, 40, 46–50). This lack includes features typical of CNS viral infection (51, 52) or its markers, such as microglial nodules, perivascular lymphocytic cuffing, focal demyelination, and intracellular viral inclusions. Microvascular, acute and subacute ischemic, and/or hemorrhagic lesions have frequently been reported in COVID-19 (4, 11, 13, 20, 26, 30, 33, 35, 36, 38, 39, 45–50, 53–62), but these are common in unselected autopsy series. With a lack, in most studies, of appropriate non-COVID-19 control cases, it has been difficult to know what brain lesions are specifically due to, or are more common in, COVID-19.

Of possible CNS entry points, both clinical and autopsy evidence has converged on the olfactory bulb (OB), with its immediate neural connection to the olfactory sensory epithelium in the nasopharynx (11, 36, 40, 63, 64). Whole or partial loss of the sense of smell is present in 60% of COVID-19 patients (64–66). The olfactory mucosa strongly expresses angiotensin-converting enzyme-2 (ACE2) and neuropilin-1, which are probable cellular access cofactors for SARS-CoV-2 (67–72). Of the reports using RT-PCR to localize SARS-CoV-2 RNA in postmortem COVID-19 brain tissue, only a few of these have assayed more than a very few brain regions. One study that assayed multiple brain regions found positive OB viral gene amplification in 8/15 (53%) while all other brain regions except midbrain were negative (40).

The intersection of COVID-19 with neurodegenerative disease is important to consider. For both bacterial pneumonia and other pandemic lower respiratory viral infections, aside from general risk factors including wintertime occurrence, older age, male sex, obesity, pre-existing cardiopulmonary conditions, and diabetes (73–93), people with age-related neurodegenerative diseases are at increased risk (94–112). COVID-19 has caused disproportionate mortality in those with dementia, and the apolipoprotein E-ε4 allele, a genetic risk factor for Alzheimer disease (AD), may be more common in subjects with severe COVID-19 disease (113–119). Possible viral etiologies for AD and Parkinson disease have been frequently debated (120–125). Post-encephalitic parkinsonism, which surged subsequent to the 1918–1919 global H1N1 influenza pandemic, is associated with substantia nigra pigmented neuron loss and neurofibrillary tangle formation but a causative linkage with the virus is still debated (126).

With direct viral brain damage seemingly uncommon in COVID-19, it appears more likely that the neurological manifestations are mostly due to systemic reactions that are common to critical illnesses and may therefore be reflected by mainly functional changes. Gene expression is a functional change that is sensitive to both local and systemic influences and may occur without accompanying alterations in cellular structure. Changes in CNS gene expression could account for much of the neurological spectrum of COVID-19.

We assessed SARS-CoV-2 genomic presence and its possible effects on histopathology, gene expression, and immune response in 42 brains from patients who died of COVID-19 in comparison with 107 subjects without COVID-19.

MATERIALS AND METHODS

Overview of Study Design and Human Subjects

The research protocols for this case-control study were approved by Institutional Review Boards for Banner Sun Health Research Institute (BSHRI) and the Mayo Clinic Florida. Written informed consent or verbal telephone consent was obtained from all participants or their legal representatives.

The majority of subjects were autopsied by the Arizona Study of Aging and Neurodegenerative Disorders (127) and Brain and Body Donation Program (AZSAND/BBDP) at BSHRI, a longitudinal clinicopathological study and biospecimen resource for normal aging and brain pathology; a subset of these were co-enrolled in the National Institute on Aging-funded Arizona Alzheimer's Disease Core Center. Ten COVID-19 subjects were recruited from Banner Health hospitals in metropolitan Phoenix and Tucson, Arizona, and autopsied at BSHRI through a separate, dedicated COVID-19 IRB protocol. Ten additional COVID-19 subjects were autopsied by the Mayo Clinic Brain Bank in Jacksonville, Florida. Inclusion criteria for all cases included presence (cases) or absence (controls) of a clinical diagnosis of COVID-19 proximal to death and/or RT-PCR detection of SARS-CoV-2 on a postmortem nasopharyngeal swab. All COVID-19 cases had died within the acute or subacute stage of their illness, not more than 6 weeks after the onset of symptoms, but comprehensive clinical records were not available for all cases. A mixture of AZSAND non-COVID-19 control subjects dying pre-pandemic or during the COVID-19 pandemic, with or without non-COVID-19 pneumonia and with or without a major neurodegenerative condition were included, allowing an exploration of the influence of these on outcomes measured in the brain. There were no exclusions for the COVID-19 cases recruited through the dedicated COVID-19 protocol at BSHRI. COVID-19 subjects died between March 1, 2020 and March 30, 2021 while control subjects died throughout 2019, 2020, and 2021.

A series of tissue investigations (Fig. 1) incorporated sets of COVID-19 and control subjects and were dependent in part on the most suitable cases that were available as the pandemic progressed. The highest priority objective and therefore the first to be undertaken was to determine the brain regional presence of SARS-CoV-2 genomic sequences. Sixteen brain regions as well as postmortem cerebrospinal fluid (CSF) and intracardiac blood serum were initially assessed with RT-qPCR. The brain regions were chosen to include potential viral

entry portals through cranial nerves (OB with closely connected regions amygdala (AMY), entorhinal area (ENT) and hippocampal CA1; pontine tegmentum in the region of the trigeminal nuclei; medulla in the region of the dorsal motor nucleus of the vagus nerve) or hematogenously (leptomeninges, choroid plexus and blood-brain-barrier-deficient median eminence of hypothalamus and area postrema of rostral dorsal medulla). Subsequent analyses, including case-control comparisons of gene expression, circulating and local cytokine concentrations, microglial reaction and neuronal markers, utilized the most appropriate additional subsets of cases and controls, and focused on the OB and the closely connected AMY.

General histopathological and viral-typical brain changes were investigated with hematoxylin and eosin (H&E) staining across all 42 cases and 107 controls by standard neuropathological examination of 25–30 brain regions.

Clinical data for AZSAND subjects were obtained from their annual standardized research assessments, including neuropsychological batteries and behavioral and movement disorders neurological assessments (127), and from abstraction of their private medical records. For the 10 COVID-19 subjects separately enrolled from hospitals in Tucson and Phoenix, as well as the 10 COVID-19 subjects enrolled by the Mayo Clinic Florida, clinical data were collected from private medical records, including from hospitals and/or medical providers' office records.

Neuropathological and Histological Analyses

For BSHRI subjects, most had whole-body autopsies while autopsies on all 10 subjects from the Mayo Clinic were restricted to the brain. The left side of each brain was fixed in neutral-buffered commercial formalin while the right side was sliced into 1-cm coronal slabs and frozen on dry ice, then stored at −80°C.

Board-certified anatomical pathologists (Pathology Specialists of Arizona, LLC and Stanford University Department of Pathology) noted the presence or absence of acute lung injury or acute pneumonia in subjects that had whole-body autopsies, and neuropathologists (T.G.B. for BSHRI and D.W.D. for Mayo Clinic Florida) performed standard neuropathological examinations, noting the presence or absence of the classical neuropathology associated with viral CNS infections or potential sequelae such as acute disseminated encephalomyelitis (ADEM), including lymphocytic leptomeningitis and encephalitis, microglial nodules, perivascular lymphocytic cuffing, focal demyelination, and viral intracellular inclusions. Also noted were any acute or subacute microscopic changes. Otherwise, the neuropathological diagnostic approach has been previously described (127). For both BSHRI and Mayo Clinic, published clinicopathological consensus criteria for neurodegenerative and cerebrovascular disease (128–140) were used when applicable, with reference to research clinical assessment results as well as pertinent private medical history. The histological sampling and staining incorporated the protocols recommended by the National Institute on Aging and Alzheimer's Association (NIA-AA) (138–140).

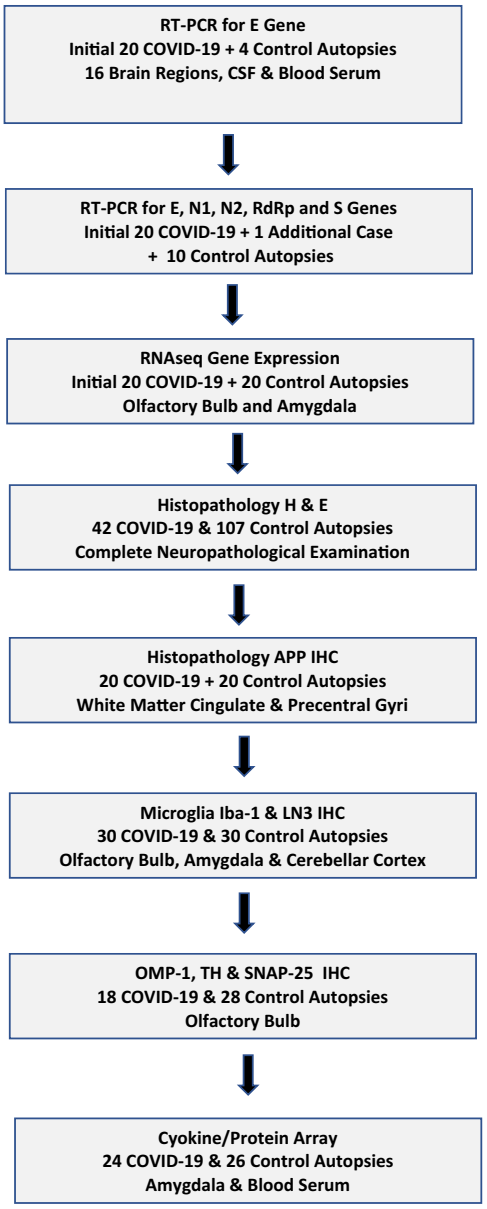

FIGURE 1. Tissue analysis flowchart. A series of tissue investigations incorporated the most suitable COVID-19 and control subjects as appropriate and was dependent in part on those cases that were available as the pandemic progressed. The highest priority objective and therefore the first to be undertaken was to determine the brain regional presence of SARS-CoV-2 genomic sequences. Subsequent analyses, including case-control comparisons of gene expression, circulating and local cytokine response, microglial reaction and neuronal markers, utilized the most appropriate additional subsets of cases and controls as they became available, and focused on the OB and the closely connected amygdala (AMY). General histopathological and viral-typical brain changes were documented with H&E staining across all 42 cases and 107 controls by standard neuropathological examination with additional immunohistochemical staining for β-amyloid precursor protein (APP) to augment sensitivity for hypoxic-ischemic changes in a subset of subjects and brain regions. IHC, immunohistochemistry; OMP-1, olfactory marker protein-1; TH, tyrosine hydroxylase; SNAP-25, synaptosomal-associated protein, 25 kDa.

Immunohistochemical stains were performed using primary antibodies listed in Table 1. Staining for β-amyloid precursor protein (APP) was done on sections of anterior cingulate gyrus with corpus callosum as well as precentral gyrus, to assist with the detection of localized white matter axonal swellings indicative of subacute and acute axonal damage, a reported finding in the brains of COVID-19 subjects (54, 55). Staining for microglia used antibodies for Iba1, a pan-microglial marker, and LN3, a marker of HLA-DR and hence "activated" microglia. OB neuronal constituents were stained (141) with antibodies to olfactory marker protein-1 (OMP-1), synaptosomal-associated protein, 25 kDa (SNAP-25), and tyrosine hydroxylase (TH). Signal development was performed as previously published with 3,3′-diaminobenzidine as chromogen (141, 142).

Staining for APP was assessed as present or absent in each section, and semi-quantitatively on a 0–3 scale. For the other immunostains, the area occupied by stained tissue elements was determined with digital image analysis (Image J software with image processing and analysis in Java: https://imagej.nih.gov/ij/). The means of the areas occupied by staining in 4 images of each brain region were used for statistical analyses, including with Mann-Whitney U-tests for ordinal variables and unpaired, 2-tailed t-tests for continuous variables as well as one-way analysis of variance with post-hoc Bonferroni-corrected pairwise significance testing or Kruskal-Wallis analysis of variance with Dunn's multiple comparisons pairwise testing. Fisher exact tests were used to test for proportional differences and Pearson or Spearman correlations for relationships between continuous or ordinal variables. The probability level for all tests was set at $p < 0.05$.

RT-qPCR Detection of SARS-CoV-2 RNA Sequences

To assess for diagnostic SARS-CoV-2 viral presence, postmortem nasopharyngeal swabs from all BSHRI cases autopsied after March 2020 were assayed using FDA EUA protocols: https://www.fda.gov/media/136818/download at Clinical Laboratory Improvement Amendments (CLIA)-approved laboratories, either operated by Sonora Quest, a division of Quest Diagnostics, or by the Stanford University Health Care Blood Center in Stanford, California.

Frozen brain samples were dissected from 16 brain regions, including OB, ENT, CA1 region of the hippocampus, AMY, temporal, frontal and primary visual neocortex, dorsal medulla in the region of the motor nucleus of the vagus nerve and area postrema, pontine tegmentum in the region of the trigeminal nuclei, substantia nigra, hypothalamus in the region of the median eminence, midportion of the thalamus, putamen at the lentiform nucleus, cerebellar cortex, choroid plexus, and leptomeninges. Cases with whole-body autopsy were sampled for frozen tissue bilaterally from the upper and lower lung lobes. Aliquots of postmortem intracardiac blood serum and postmortem intraventricular CSF were also assayed.

RNA was extracted from 20 mg of frozen brain and lung tissue or 200–250 μL of blood serum and CSF using Qiagen RNeasy Plus Mini Kits (Cat # 74134 for tissue and 217204 for blood serum and CSF) following the manufacturer's instructions and eluted in 50 μL of RNAse-free water. SARS-CoV-2 RNA was detected using previously described primer and probe sequences (Table 2) targeting the envelope (E) (143), RNA-dependent RNA polymerase (RdRp) (143), and spike protein (S) (144) genes. N1, N2, and RNase P sequences were obtained from CDC and FDA websites: https://www.fda.gov/media/134922/download; https://www.cdc.gov/coronavirus/2019-ncov/lab/rt-pcr-panel-primer-probes.html.

RNase P and actin primers and probes were used as housekeeping gene amplification controls. RT-qPCR was performed in duplicate in separate wells with a 20-μL volume containing 4 μL of RNA (80–160 ng) and 5 μL of 4× Taqpath One-Step RT-qPCR Master Mix (Cat # A15299 Life Technologies, Carlsbad, CA) on Bio-Rad CFX Connect. For blood se-

TABLE 1. Primary Antibodies, Dilutions and Pretreatments Used for Histology Studies

Antibody Target	Abbreviation	Clone	Supplier/Cat. #	Dilutions/Pretreatment
CD3, T-lymphocytes	CD3	F7.2.38	Dako/Agilent M725401-2	1:100; steam in Tris/EDTA, pH9
CD20, B-lymphocytes	CD20	L26	Dako/Agilent M075501-2	1:1000; steam in citrate pH 6
CD 68, macrophages	CD68	KP1	Dako/Agilent M081401-2	1:1000: steam in dH20
β-amyloid precursor protein	APP	22C11	Millipore MAB348	1:3000; steam in dH20
Ionized calcium binding adaptor molecule 1	Iba1	polyclonal	Wako 016-20001	1:5000; boiling EDTA
HLA-DR	LN3	LN3	Abcam 166777	1:10 000; boiling EDTA
Olfactory marker protein-1	OMP-1	polyclonal	Novus NB110-74751	1:2000; boiling citrate
Synaptosomal-associated *protein, 25kDa*	SNAP-25	polyclonal	Sigma S9684	1:5000; Formic Acid
Tyrosine hydroxylase	TH	TH-16	Sigma T2928	1:3000; boiling citrate

TABLE 2. Gene Sequences for Primers and Probes Used for RT-qPCR

Name	Sequence (5′-3′)	Conc. (nM)	Vendor	Cat. #
E_Sarbeco_F	ACAGGTACGTTAATAGTTAATAGCGT	800	Life Tech.	A15612
E_Sarbeco_R	ATATTGCAGCAGTACGCACACA	800	Life Tech.	A15612
E_Sarbeco_P1	FAM-ACA CTA GCC ATC CTT ACT GCG CTT CG-QSY	400	Life Tech.	4482777
RdRp_SARSr-F	GTGARATGGTCATGTGTGGCGG	600	Life Tech.	A15612
RdRp_SARSr-R	CARATGTTAAASACACTATTAGCATA	800	Life Tech.	A15612
RdRp_SARSr-P2	FAM-CAGGTGGAACCTCATCAGGAGATGC-BBQ	100	Life Tech.	4482777
2019-nCoV_N1-F	GAC CCC AAA ATC AGC GAA AT	500	Int. DNA Tech.	10006830
2019-nCoV_N1-R	TCT GGT TAC TGC CAG TTG AAT CTG	500	Int. DNA Tech.	10006831
2019-nCoV_N1-P	FAM-ACC CCG CAT TAC GTT TGG TGG ACC-BHQ1	125	Int. DNA Tech.	10006832
2019-nCoV_N2-F	TTA CAA ACA TTG GCC GCA AA	500	Int. DNA Tech.	10006833
2019-nCoV_N2-R	GCG CGA CAT TCC GAA GAA	500	Int. DNA Tech.	10006834
2019-nCoV_N2-P	FAM-ACA ATT TGC CCC CAG CGC TTC AG-BHQ1	125	Int. DNA Tech.	10006835
S Gene-Fwd	TCAACTCAGGACTTGTTCTTAC	360	Life Tech.	A15612
S Gene-Rev	TGGTAGGACAGGGTTATCAAAC	360	Life Tech.	A15612
S Gene-Probe	TGGTCCCAGAGACATGTATAGCAT-BHQ1	80	Life Tech.	4482777
ACTB_F	GACGTGGACATCCGCAAAGAC	800	Life Tech.	A15612
ACTB_R	CAGGTCAGCTCAGGCAGGAA	800	Life Tech.	A15612
ACTB_P1	FAM-TGCTGTCTGGCGGCACCACCATGTACC-QSY	400	Life Tech.	4482777
Rnase P_F	AGA TTT GGA CCT GCG AGC G	500	Int. DNA Tech.	10006836
Rnase P_R	GAG CGG CTG TCT CCA CAA GT	500	Int. DNA Tech.	10006837
Rnase P_P	FAM-TTC TGA CCT GAA GGC TCT GCG CG-BHQ-1	125	Int. DNA Tech.	10006838

E, envelope (E) gene; ACTB, actin beta; RNase P, ribonucleus P; F, forward; R, reverse; Conc, concentration of primer used; Life Tech., Life Technologies; Int. DNA Tech., Integrated DNA Technologies.

rum and CSF, due to low sample RNA concentrations, 4 μL of undiluted RNA was used, with a maximum of 160 ng per aliquot. Positive gene sequence presence was defined alternatively as a Ct value equal to or less than 40, or equal to or less than 35, for E, RdRp, and S genes. Both N1 and N2 genes were required to be at or below the same thresholds in order for the sample to be classified as positive. Inconsistent results, e.g. when one of the duplicates amplified but not the other, were repeated in new duplicate samples and results were only accepted as positive with at least one duplicate.

Positive controls were included in each RT-PCR run; these included a mixture of synthetic SARS-CoV-2 RNA sequences (RNA transcripts for 5 gene targets, E, N, ORF1ab, RdRp, and S genes; Cat # COV019 Bio-Rad Labs, Hercules, CA), as well as a frozen lung RNA sample from a COVID-19 decedent previously shown to be reliably positive. The number of E gene copies per brain or lung sample were estimated by interpolation on a standard curve created with serial dilutions of 1:1 synthetic SARS-CoV-2 RNA (successive dilutions were each 2-fold more dilute).

To evaluate assay validity, RNA aliquots from each of 5 study subjects, with a total of 30 samples, including positive and negative samples of OB, dorsal medulla and lung, were analyzed blinded to diagnosis and previous RT-PCR results using similar RT-PCR methods for detection of the E gene at the Stanford University Health Care Blood Center, with complete agreement on positive versus negative results for all anatomical sites and subjects.

Gene Expression Analysis

RNA was extracted as detailed above; mean RNA integrity number (RIN) was greater than 9.0. Sequencing libraries were prepared with 100 ng of total RNA using Illumina's TruSeq Stranded Total RNA library prep approach (Illumina, Inc., San Diego, CA) following the manufacturer's protocol. The final library was sequenced by 2 × 100 bp paired-end sequencing on an Illumina NovaSeq6000.

After sequencing, FASTQs files were aligned to the Human Reference Genome HG38 using STAR (145), and summarized at the gene level with HTSeq. Quality controls were conducted using MultiQC software (146) and principal component analysis. Samples with RIN <4, total number of reads <20M, and uniquely mapped reads <70% were excluded from the downstream analysis. Genes with a total count of <10 were excluded and normalization was performed using DEseq2. Differential gene expression was calculated between the COVID-19 samples and the controls using DEseq2, adjusting for age at death, sex, brain tissue source (BSHRI or Mayo Clinic), and neuropathologically determined presence or absence of a diagnostic level of a major neurodegenerative disease. Genes with a false discovery rate (FDR) p value smaller than 0.05 were considered differentially expressed genes (DEGs). Pathway analysis was conducted on the DEGs using a hypergeometric statistic referencing the REACTOME database as implemented in the *clusterProfiler* R package.

Lists of cell-specific genes were generated from a brain single-nucleus RNA sequencing dataset from the dorsolateral

prefrontal cortex (147) that included AD cases and non-demented controls (total: n = 48). Data were downloaded from the Accelerated Medicine Partnership-AD portal (AMP-AD; accession number syn18485175). The filtered dataset consisted of a total of 70 634 droplet-based single-nuclei and 17 352 genes from: astrocytes (Ast), endothelial cells (End), excitatory neurons (Ex), inhibitory neurons (In), microglia (Mic), oligodendrocytes (Oli), oligodendrocyte precursor cells (Opc), and pericytes (Per). After excluding the AD samples, the data matrix was imported into Seurat (148) and normalized using the function "NormalizeData" with the option "LogNormalize," using a scale factor of 10 000. Then, each gene was assigned to a cell class modeling a linear regression where the expression levels were the dependent variable and the cell type the predictors, adjusting for sex, age, and post-mortem interval. A transcript was assigned to a cell type when: (1) the adjusted p values (FDR) were $p < 0.05$, and (2) the regression coefficient of the enriched cell type had a ratio >1.81 with the second enriched cell type. The cutoff was established after testing all coefficient ratios from 1 to 5 until the variation of the number of unclassified genes stabilized to under 0.5%. We obtained a list of 5641 cell-type-specific genes, which were used as gene sets to run enrichment analysis on the DEGs. The analysis was conducted using the R function *enrichment* (R package *bc3net*) adjusting the results for multiple testing with the FDR method.

WGCNA analysis was done to detect relevant co-expression networks associated with COVID-19 status (149). The count table was normalized with the *voom* method (150), and adjusted for confounding factors as in the differential expression analysis using the function *removeBatchEffect* as implemented in *limma* (151). Genes with <5 total counts per minute were removed from the dataset. Finally, 50% of the most variable genes were retained after computing the median absolute deviation with the goal of excluding genes with low variability, minimizing the noise in the co-expression networks. Soft-thresholding power (β) was computed using the *pickSoftThreshold* function. Then, the values were plotted against the scale-free fit index and selected for the lowest power for which the scale-free topology fit index curve flattens out upon reaching a $r^2 = 0.900$ (152). A signed co-expression network was generated and identified the resulting clusters using the function *blockwiseModules* with the following parameters: *TOMtype*: "signed," *minimum module size* = 30, *mergeCutHeight* = 0.30, *deepSplit* = 2; reassign threshold = 1.0^{-06}, and *pamRespectsDendro* = "TRUE." We computed the eigengene values for each individual and module by singular value decomposition (153). The eigengenes were compared by module between COVID-19-positive and controls using a linear model as implemented in *limma*, adjusting the p values for multiple testing by accounting for the number of modules using the FDR method. Covariates were not included in the model since we adjusted the expression values matrix. Gene ontology (GO) enrichment analysis was performed on the differentially expressed modules associated with COVID-19 status by the means of the R-package *enRichment*, using as background the intersection of given genes and genes present in GO. P values of the GO enrichment analysis were adjusted using the Bonferroni method. The enrichment for genes specifically expressed in certain cell types was conducted using the above-described cell specific markers by means of a hypergeometric test as implemented in the R function *enrichment*. Finally, the top hub genes in the co-expression modules were identified using the function *chooseTopHubInEachModule* as implemented in the WGCNA package.

Cytokine and Protein Arrays

Frozen brain samples, approximately 30 mg, were dissected from the estimated region of the cortical nucleus/periamygdalar region of the AMY. Tissue was homogenized for protein extraction in RIPA buffer plus Protein Inhibitor Cocktail using an OmniTH tissue grinder and centrifuged for 30 minutes at 4 C at 18 000 rpm (40 000×*g*). Micro BCA protein assays were used to calculate the protein concentrations and the homogenates were stored at −80°C until testing. Blood was taken postmortem by intracardiac puncture and placed in VACUETTE Serum Clot Activator Tubes (Greiner Bio-One; VWR CAT# 95057-393). CSF was taken postmortem from the lateral cerebral ventricles. Both types of biofluids were centrifuged at 2000*g* for 10 minutes at 24°C. Aliquots of each (0.5 mL) were frozen at −70 to −80°C until used.

Commercial Quantibody Human Cytokine Array kits (QAH-CYT-1; RayBiotech, Inc., Norcross, GA) were used to detect 20 human cytokines/proteins (CCL2, CCL3, CCL4, CCL5, CSF2, CXCL1, CXCL2, CXCL3, CXCL8, IFNG, IL10, IL12A, IL13, IL1A, IL1B, IL2, IL4, IL5, IL6, MMP9, TNF, and VEGFA). AMY protein homogenates were assayed at a 2000 µg/mL concentration and at 1:1 dilution while serum and CSF samples were assayed undiluted. Samples and standards were diluted in the sample diluent provided with each kit. Biotinylated antibodies were detected with Cy3-coated streptavidin and analyzed with an Axon Gene Pix 4200 A laser scanner (Molecular Devices, Silicon Valley, CA) at a wavelength of 555 nm and settings of 450, 550 and 650 pmt. Standard curves were analyzed by regression based on linear and logarithmic transformations of the data. The results of any one assay were based on the same PMT readings and data transformation for all cytokines if the correlation coefficient was ≥0.90 for the standard curve. Data not meeting this latter criterion were excluded.

RESULTS

Demographic, Pneumonia, and Neuropathological Characteristics of Subjects

A total of 149 autopsied subjects were included (Table 3). The mean age of the COVID-19 cases was significantly lower than that of the controls ($p = 0.02$), although both groups were of advanced age with medians over 80. Subjects were 100% Caucasian; 5 were of Hispanic ethnicity. Of 28 COVID-19 cases with whole-body autopsy including lungs, 25 had microscopic changes consistent with acute lung injury and/or acute bronchopneumonia. Of the 3 without pneumonia, 1 died of acute myocardial infarction, 1 died of likely congestive heart failure causing pulmonary edema, and 1 died of

TABLE 3. Demographic, Pneumonia, and Neuropathological Characteristics of All Subjects

Group	Age Median (Range)	Female N (%)	Acute Lung Injury or Acute Pneumonia N (%)	ApoE-ε4 N (%)	Major Neuropath Dx N (%)	Braak Neurofibrillary Stage Median (Range)	Thal Amyloid Phase Median (Range)
COVID-19 n = 42	81.5 (38–97)*	21 (50%)	23/26 (88%)	8/24 (33%)	24 (57%)	4 (0–6)	3 (0–5)
Control n = 107	87 (52–104)	83 (57%)	64/101 (63%)	31/101 (31%)	69 (47%)	4 (1–6)	3 (0–5)

*Significantly different p = 0.02.
A major neuropathological diagnosis is defined as the presence of Alzheimer disease dementia, vascular dementia, hippocampal sclerosis, progressive supranuclear palsy, Parkinson's disease, multiple system atrophy, dementia with Lewy bodies, diffuse Lewy body disease, or frontotemporal lobar degeneration with TDP-43 proteinopathy. Missing data for lungs are due to not having lungs included in the autopsy. Missing data for ApoE are for determinations not done. ApoE-ε4 = heterozygous or homozygous.

TABLE 4. Demographic, Pneumonia, and Neuropathological Characteristics of Consecutive AZSAND Subjects Autopsied in the Arizona Pandemic Period From June 2020 Through March 30, 2021

Group	Age Median (Range)	Female N (%)	Acute Lung Injury or Acute Pneumonia N (%)	ApoE-ε4 N (%)	Major Neuropath Dx N (%)	Braak Neurofibrillary Stage Median (Range)	Thal Amyloid Phase Median (Range)
COVID-19 N = 22	85.5 (66–96)	11/22 (50%)	13/16* (81%)	6/22 (27%)	13/22 (59%)	4 (0–6)	3 (0–5)
Control N = 52	85.9 (52–104)	20/52 (38.5%)	29/41 (71%)	16/52 (31%)	32/52 (61.5%)	4 (1–6)	3 (0–5)

*Significantly different p = 0.004.
See Table 3 for explanation of columns.

complications of an aggressive meningioma with extensive dural, brain and bone invasion.

COVID-19 cases all occurred before April 2021, prior to the introduction of the Delta variant to North America. Variant status was not determined by sequencing. Of chosen pre-pandemic and pandemic-era control subjects (the latter defined as being negative to postmortem nasopharyngeal swab RT-PCR) with a whole-body autopsy and postmortem lung examination, 63% had acute pneumonia; the proportion of control subjects with acute pneumonia was deliberately enhanced for comparative purposes. The proportions with the apolipoprotein E-ε4 allele did not differ between COVID-19 and control groups. There were proportionately more males and more major neuropathological diagnoses in the COVID-19 group but the differences were not significant (Fisher exact test, p = 0.48 and 0.30, respectively). Braak neurofibrillary stage and Thal amyloid phase did not differ between groups.

As pre-pandemic AZSAND autopsy control subjects listed in Table 3 were not chosen randomly, and the subjects derived from the Mayo Clinic IRB protocol and the dedicated COVID-19 Banner Health IRB protocol had differing origins, a comparison was also made of consecutive AZSAND autopsies throughout the pandemic period from June 2020 through March 30, 2021 (Table 4). Of 74 consecutive autopsies, 22 (30%) had SARS-CoV-2 detected on their postmortem nasopharyngeal swabs. The age difference seen with the full subject set (Table 3) was no longer present. The male predominance among AZSAND COVID-19 cases was more pronounced (61.5%) than in the full subject set but still did not reach significance (p = 0.44). The COVID-19 group had a significantly higher proportion with acute lung injury or acute pneumonia (p = 0.004). The groups had similar percentages with a major neuropathological diagnosis and equal median scores for Braak stage and Thal amyloid phase. See Supplementary Data Table S1 for more detailed data on all participants.

Brain Regional Presence of SARS-CoV-2 Gene Sequences

We published in preprint form (154) our initial results derived from screening with RT-qPCR for the E gene in 16 brain regions, as well as postmortem serum and CSF, of the first 20 COVID-19 autopsies as well as 4 control cases (Supplementary Data Table S2). Four COVID-19 cases (20%) were considered positive with a Ct threshold less than or equal to 40, with 2 positive cases in the OB and 1 positive case each in AMY, ENT, middle temporal gyrus, middle frontal gyrus, dorsal medulla, and leptomeninges, for a total positivity rate of 7/320 (2.5%) tested brain regions. The brain region with the highest estimated viral load by cycle number, for both the BSHRI and Mayo Clinic cases, was the OB. All 9 of the assayed BSHRI COVID-19 disease cases with whole-body autopsy showed above-threshold amplification of the SARS-CoV-2 E gene sequence in their lung samples. Interpolating from a synthetic SARS-CoV-2 standard concentration curve

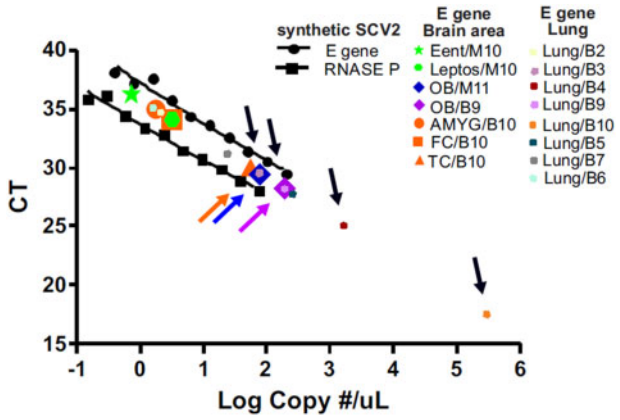

FIGURE 2. Standard curve for obtaining estimated SARS-CoV-2 RNA copy numbers in samples, constructed with serial dilutions of commercially obtained synthetic SARS-CoV-2 RNA. Black circles are from synthetic E gene RNA dilutions; black squares are from synthetic RNAse P gene RNA dilutions. Also plotted are Ct values for subject samples that were positive for threshold amplification (≤Ct 35) for E gene RNA (colored symbols, larger symbols are for brain samples, symbols for lung samples are smaller; some symbols are superimposed on others). The highest copy numbers were obtained from lung samples (downward-pointing arrows show lung samples with higher Ct values), olfactory bulb samples ([OB], arrows pointing to diamond symbols), and a temporal cortex sample ([TC], arrow pointing to triangle symbol). Ent, entorhinal area; Leptos, leptomeninges; AMYG, amygdala; FC, frontal cortex; B2-B7, B9, B10 are consecutive BSHRI cases that included lungs in the autopsy. M10 and M11 are Mayo Clinic cases. See Supplementary Data Table S1 for case details.

(Fig. 2), the highest brain region viral load estimate was approximately 189 copies of the E gene sequence, in the OB of case B9 (BSHRI case 20-67), while the lowest load was 0.7 copies, in the ENT of Mayo case 10. Brain loads were generally much lower than those in the lungs, where the highest viral load was estimated at 300 000 copies. None of the postmortem cardiac blood serum and CSF samples, assayed in 8 and 9 BSHRI cases, respectively, had E gene amplification meeting the Ct 40 threshold. Housekeeping gene (RNAse P and actin) amplification was adequate for all samples and serial amplified dilutions for RNAse P are plotted in Figure 2. Threshold E gene amplification was not achieved in any of the lung, brain, or biofluid samples from the 4 AZSAND non-COVID-19 control cases.

Since our preprint report, additional RT-qPCR assays on frozen samples of OB, AMY and ENT were performed, repeating the E gene assays and adding assays for the N1, N2, RdRp, and S genes (Table 2; Supplementary Data Table S3), and adding one additional COVID-19 case for a total of 21 evaluated. Positivity was again defined as Ct less than or equal to 40. These assays replicated the 2 positive results in OB and the 1 positive result for AMY, and detected SARS-CoV-2 RNA in OB from additional cases, giving a new total of 8/21 SARS-CoV-2-positive cases in OB (Table 5) and 8/21 cases positive in at least one brain region overall. There were no new positive results for AMY or ENT. All of the 9 BSHRI COVID-19 cases assayed tested positive for all genes in their lung samples (Supplementary Data Table S3). None of 4 control cases (3 with and 1 without non-COVID-19 pneumonia) tested positive for the E gene in any of the 16 brain regions, CSF or serum and none of 10 controls (all with non-COVID-19 pneumonia) tested positive for E, N1/N2, RdRp, or S genes in samples of lung, OB, AMY, or ENT.

With an alternate Ct cutoff of 35, the results of the additional SARS-CoV-2 gene sequence screening gave 5 (25%) positive COVID-19 cases. For all Ct values, see Supplementary Data Table S3.

TABLE 5. RT-PCR-Positive Brain Regions by Subject and SARS-CoV-2 Gene Target

Subject	Region	E Ct	N1 Ct	N2 Ct	RdRp Ct	S Ct
20–67	OB	28.21	28.26	28.53	27.89	28.58
20–72	OB	40.74	36.37	37.33	Neg	37.35
20–74	OB	32.37	35.07	35.69	ND	35.99
Mayo 4	OB	Neg	37.91	39.12	Neg	Neg
Mayo 6	OB	Neg	36.75	39.58	Neg	39.07
Mayo 8	OB	37.32	38.15	37.24	Neg	36.94
Mayo 10	OB	Neg	33.39	34.62	ND	33.76
Mayo 11*	OB	29.46	Neg	Neg	Neg	ND
20–72	AMY	34.23	32.56	34.17	Neg	34.27
Mayo 10	ENT	36.23	Neg	Neg	ND	Neg

*For M11 OB, a second RNA isolation was required but with limited remaining tissue. As a result, less RNA was available for the N1, N2, RdRp, and S assays than was used for the other cases in the table.

An initial survey targeted the E gene in 16 brain regions as well as blood serum and CSF in 20 COVID-19 cases. Subsequently, the N1, N2, RdRp, and S genes were targeted in the olfactory bulb (OB), amygdala (AMY), and entorhinal area (ENT). Samples with Ct of 40 or lower were considered positive; N1 and N2 genes were both required to be positive in order for the sample to be considered positive. Control cases were not positive in any brain region. Neg, no amplification; ND, not done. See Supplementary Data Tables S2 and S3 for complete results.

Case-Control Gene Expression Differences

Cases and Controls Used for Gene Expression Analysis

COVID-19 cases used for gene expression analysis were the same original 20 cases as those used to map the gene regional presence of SARS-CoV-2 viral sequences; control cases were non-COVID-19 AZSAND subjects autopsied in 2018 and 2019, prior to the COVID-19 pandemic (Table 6; Supplementary Data Table S1). The mean age of the COVID-19 cases was significantly lower than that of the controls ($p = 0.009$) but both groups were elderly (medians of 77 and 84, respectively). Of the 9 COVID-19 cases with whole-body autopsy including lungs, all 9 had microscopic changes consistent with acute lung injury and/or acute bronchopneumonia. Of control subjects with a postmortem lung examination, 9/20 (45%) had acute pneumonia. The proportions of male sex, with the apolipoprotein E-ε4 allele, or with a major neuropathological diagnosis did not significantly differ between COVID-19 and control groups; median Braak neurofibrillary stage and Thal amyloid phase did not differ between groups.

TABLE 6. Demographic, Pneumonia, and Neuropathological Characteristics of COVID-19 and Control Cases Used for Initial RT-PCR Brain Regional E Gene Detection (COVID-19 Cases Only) and Gene Expression Analyses

Group	Age Median (Range)	Female N (%)	Acute Lung Injury or Acute Pneumonitis N (%)	ApoE-ε4 N (%)	Major Neuropath Dx N (%)	Braak Neurofibrillary Stage Median (Range)	Thal Amyloid Phase Median (Range)
COVID-19 N = 20	77 (38–93)*	9/20 (45%)	9/9 (100%)	3/10 (30%)	12/20 (60%)	4 (0–6)	3 (0–5)
Control N = 20	84 (71–100)	10/20 (50%)	9/20 (45%)	5/19 (26%)	11/20 (55%)	4 (2–6)	3 (0–5)

*Two-tailed, unpaired t-test p = 0.009.
See Table 3 for explanation of column titles.

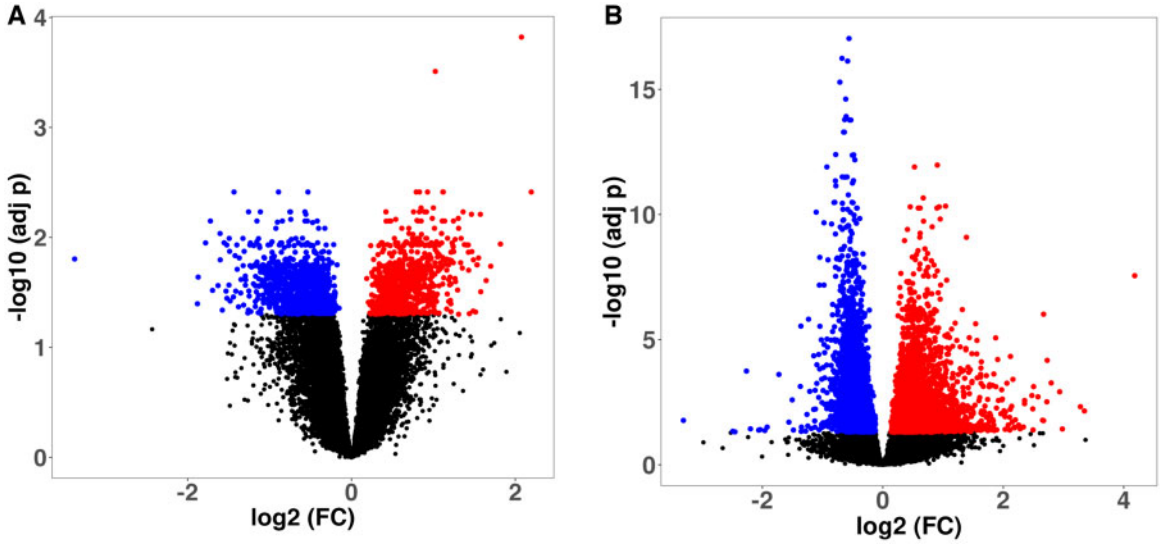

FIGURE 3. Volcano plot showing the differential expression analysis results comparing COVID-19 cases versus controls in amygdala **(A)** and olfactory bulb **(B)**. Upper points represent genes that had significantly different expression in COVID-19 as compared to controls. Genes on left and right were downregulated and upregulated, respectively, in COVID-19 cases (FDR $p < 0.05$).

The OB and AMY were chosen for comprehensive RNAseq gene expression analyses because of the high prevalence of SARS-CoV-2 genomic sequences in OB in COVID-19 cases, and because of the strong, monosynaptic neuroanatomical connections of the OB with AMY.

Differential Gene Expression in Olfactory Bulb and Amygdala

Results have previously been partially presented in preprint form (155). After removing low-quality RNA samples, the final AMY sample size was 36, of which 18 were from COVID-19 cases and 18 were from controls. For OB, all 40 samples had adequate RNA quality (20 COVID-19 cases and 20 controls). The samples had a total of 40.2 M reads (range: 20.1–235.6 M), with an average percentage of uniquely mapped reads of 84.3% (range: 72.8%-90.3%). After analysis, including adjustment for sex, age, RIN, presence or absence of a major neurodegenerative disease, and origin of subjects (Mayo vs BSHRI), we obtained 728 DEGs in AMY (794 upregulated and 934 downregulated) and 5405 DEGs (2546 upregulated and 2859 downregulated) in OB (Fig. 3; Supplementary Data Tables S4 and S5). The most highly significant expression alterations in AMY were *IFI6*, *PPP1R13L*, and *PFDN4*, whereas *UBQLN2*, *CLCNA*, and *MAPK1* were the most significant genes in OBT. The 9 genes with the greatest expression differences in AMY and OB in terms of normalized count differences, are shown in Figure 4.

Surprisingly, when comparing gene expression in COVID-19 OB samples that were positive (n = 8) or negative (n = 12) for SARS-CoV-2 viral genomic sequences, there were only 5 DEGs, *B2M*, *SEC16A*, *OASL*, *EPN3*, and *RPL27* (Figs. 5 and 6). Also, comparison of control subjects with and without autopsy-proven acute pneumonia found only 1 and 2 DEGs in OB and AMY, respectively (results not shown).

Pathway analysis revealed differential processes associated with AMY and OBT. Notable changes in AMY were enrichment of immune pathways, including interferon signaling and the toll like receptor cascade, as well as synaptic pathways (Fig. 7). In OB, the most upregulated pathways were related to

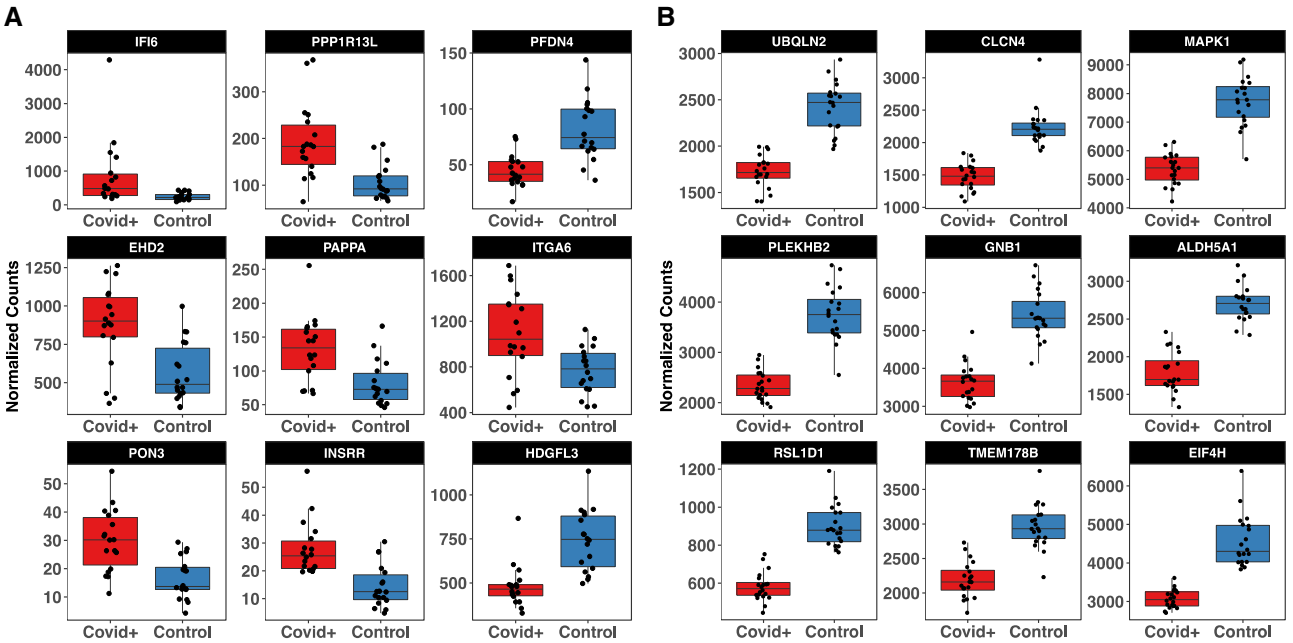

FIGURE 4. The 9 genes with the greatest expression differences in amygdala **(A)** and olfactory bulb **(B).**

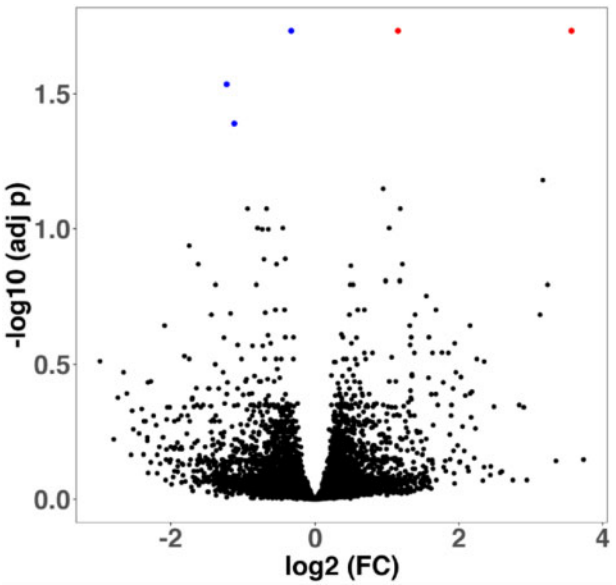

FIGURE 5. Volcano plot showing the differential expression analysis results comparing OB in COVID-19 cases that were RT-PCR-positive (right side) or negative (left side) for SARS-CoV-2 RNA sequences. Uppermost 5 points represent genes that had significantly different expression in COVID-19 as compared to controls. All other genes were not differentially expressed.

olfactory signaling, collagen/extracellular matrix modification, and integrin and immunomodulatory cellular interactions, while in both regions, synaptic and neuronal pathways were downregulated (Supplementary Data Tables S6 and S7).

Cell-specific gene enrichment across DEGs revealed overrepresentation of astrocyte (Ast) and endothelial (End) associated genes in AMY (Fig. 8); on separate analyses for upregulated and downregulated DEGs, there was overrepresentation of Ast, End and pericyte (Per) in upregulated genes and enrichment of excitatory (Ex) and inhibitory (In) neurons in the downregulated gene set. In OB, there was a significant cell-specific enrichment of End and Per among upregulated genes, and enrichment of Ex in the downregulated genes.

WGCNA Analysis

Six co-expression modules were obtained in AMY with the number of genes in each module ranging from 281 (red module) to 2947 (turquoise). After eigengene extraction and differential analysis, no modules were differentially expressed between COVID-19 and controls in AMY (results not shown). In OB, 15 co-expression modules were obtained (Fig. 9A) with the number of genes in each module ranging from 39 (midnight blue) to 1904 (turquoise). Eleven modules were differentially expressed between COVID-19 and control (Fig. 9B), with the top modules being black (downregulated in COVID-19) and red (upregulated), both with FDR = 1.68^{-11}. Gene ontology (GO) and cell enrichment analysis was performed on these 11 modules, finding GO enriched classes in 8 of the modules (Supplementary Data Table S8). The top 2 modules (black and red) were enriched for ribosome/RNA metabolism and cilium/taste, respectively. Other modules were enriched for development/angiogenesis (green, upregulated, and enriched for End and Per), immune system (tan, upregulated), and synaptic signaling (green-yellow and turquoise, both downregulated and enriched for neuronal cell genes). The 2 synaptic modules were not related to each other despite a similar functional enrichment. The summary of the WGCNA

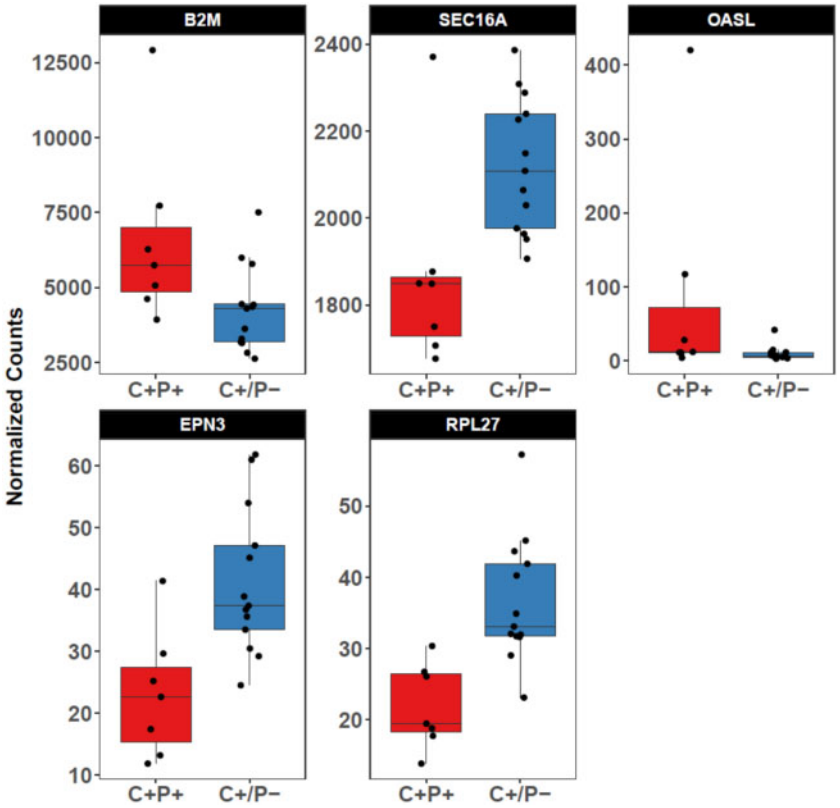

FIGURE 6. The 5 genes that were differentially expressed in the OB on the basis of being RT-PCR-positive or negative for SARS-CoV-2 genomic sequences. C+/P+, COVID-19 PCR-positive; C+/P−, COVID-19 PCR-negative.

analysis, including modules, GO and cell-specific gene enrichment, and a list of the hub genes are shown in Table 7.

Case-Control Histopathology Comparison

Attributable Histopathology and Typical Viral Histopathology

As mentioned above, there was not a significant difference between COVID-19 cases and controls in the proportions with a major neurodegenerative disease diagnosis or in their AD-related neuropathology.

Only 2 subjects had clinical and postmortem findings that were probably attributable, by temporal association, to their terminal COVID-19 illness (154). One Mayo Clinic case (Mayo 10) had acute encephalitis, with transtentorial herniation, acute hemorrhages of the temporal lobe, thalamus and pons, and neuropil infiltration by B- and T-lymphocytes and macrophages (Fig. 10A–F); the ENT was RT-PCR-positive for SARS-CoV-2. One BSHRI subject (20–40) had a large acute middle cerebral artery territory ischemic and hemorrhagic infarction (Fig. 10G–I) that was clinically documented to have occurred several days after the clinical onset of his COVID-19 disease, and was accompanied by bilateral lower extremity arterial thromboses; no brain region from this case was RT-PCR-positive.

Overall, acute or subacute infarctions and/or acute hypoxic-ischemic microscopic changes were seen in 4/42 (9.5%) of the COVID-19 cases compared to 11/107 (10.3%) of control cases (ns). Acute hemorrhages or microhemorrhages were present in 4/42 COVID-19 cases (9.5%) and 3/107 (2.8%) of the control cases (not significantly different).

No intracytoplasmic or intranuclear viral inclusions were seen in any of the cases, including the COVID-19 case with acute encephalitis. Two COVID-19 cases had 1 and 2 microglial nodules, both in the caudal dorsolateral medulla, but one of these (20–45) was not RT-PCR-positive for any SARS-CoV-2 gene in any brain region and the other (Brodmann 21-04) was only positive for the S gene, only for one replicate and only in the OB. No control case had microglial nodules. Significant perivascular cuffing with mononuclear cells was only seen in the Mayo Clinic case 10 with acute encephalitis. Definite perivascular cuffing was not seen in any of the paraffin-embedded, H&E-stained sections from other cases but in thick (80 μm) large-format sections encompassing entire cerebral lobes, occasional blood vessels in the centrum ovale had sparse to moderate cuffing (154). However, on further examination of additional cases this was seen in almost all cases and controls. These thick, large-format sections were only available for the BSHRI autopsies. Perivascular demyelination suggestive of ADEM was not seen in any case or control.

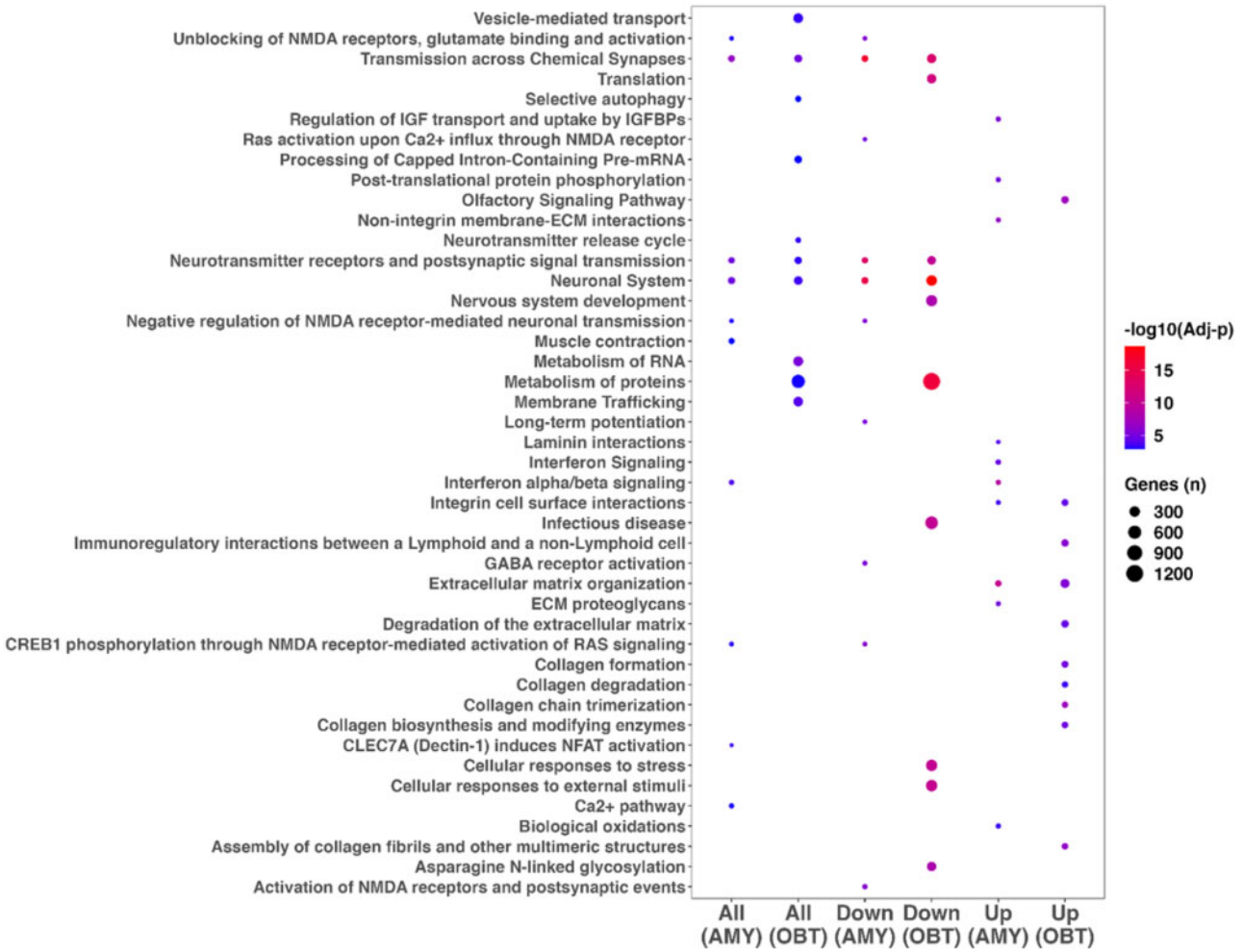

FIGURE 7. The top 10 pathways enriched in amygdala and olfactory bulb. All: all DEGs are shown regardless of up- or downregulation. Up: DEGs upregulated in COVID-19 subjects. Down: DEGs downregulated in COVID-19 subjects.

β-Amyloid Precursor Protein White Matter Staining in COVID-19 and Control Cases

As immunohistochemical stains for APP have been suggested to be a "signature" change of hypoxic leukoencephalopathy and COVID-19 brain disease (54, 55), we compared the prevalence and intensity of white matter APP staining in subsets of COVID-19 and control cases (156) (see Supplementary Data Table S1 for subject details). COVID-19 cases were younger (77.5; SD 2.9) than non-COVID-19 cases (84.0; SD 2.0); the difference was borderline significant ($p = 0.07$). Males made up 11/20 and 10/20 of the COVID-19 and non-COVID-19 cases, respectively (ns). Both COVID-19 and non-COVID-19 cases had a wide range of neuropathological diagnoses. Ten non-COVID-19 control cases had autopsy-validated acute pneumonia while 10 did not.

Figure 11 shows photomicrographs of APP staining in COVID-19 and non-COVID-19 control cases. Positive APP white matter staining was seen in at least 1 of the 2 brain regions in 14/20 COVID-19 cases and in 12/20 of the non-COVID-19 control cases (ns). Cases were positive in the precentral gyrus in 11/20 COVID-19 and 5/20 control cases (ns) while in the cingulate gyrus the ratios were 12/20 and 10/20, respectively (ns).

Comparing density scores from both brain regions combined, the mean scores for COVID-19 cases were higher than those for controls of both types together (0.91 vs 0.44, Mann-Whitney $p = 0.026$) but not significantly different (0.91 vs 0.60, $p = 0.35$) when restricting to controls with pneumonia. Region-specific pairwise scores were not significantly different between COVID-19 and controls of both types (Kruskal-Wallis analysis of variance with Dunn's multiple comparisons pair-wise testing). In both brain regions, scores were not significantly different between BSHRI and Mayo Clinic COVID-19 cases. Among control cases, when considering both brain regions together, cases with pneumonia had significantly higher scores (0.60 vs 0.27, Mann-Whitney $p = 0.044$).

When cases were divided by the presence or absence of a major neuropathologically defined neurodegenerative disorder, there were no significant differences in APP scores between the 2 groups, either when restricting to one brain region or when scores from both brain regions were grouped. When

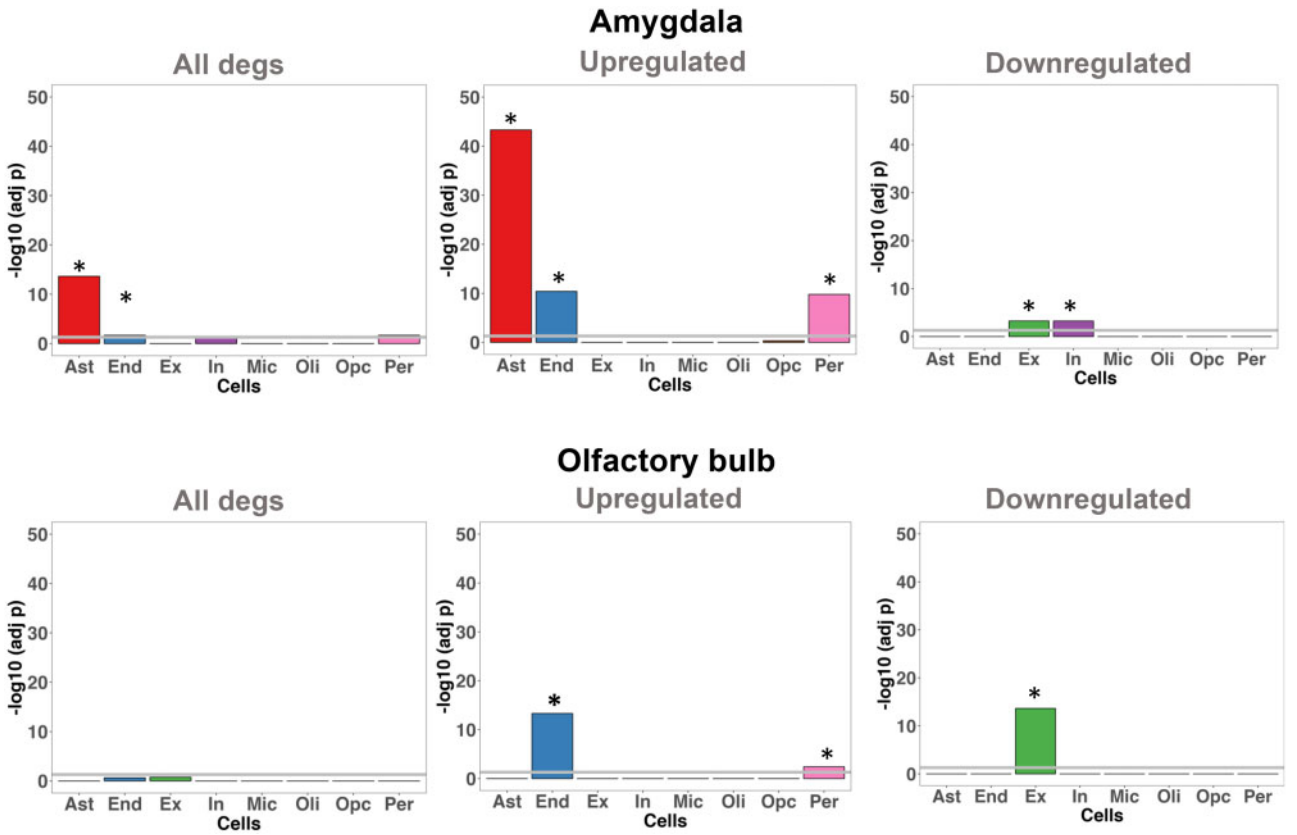

FIGURE 8. Cell-specific gene enrichment among DEGs in amygdala and olfactory bulb. Gene classes significantly enriched are indicated with an asterisk (FDR < 0.05). Ast, astrocytes; END, endothelial cells; Ex, excitatory neuron; In, inhibitory neuron; Mic, microglia; Oli, oligodendroglia; Opc, oligodendroglial precursor cells; Per, pericytes.

APP scores from cases and controls in both areas were combined, males had significantly greater scores than females (0.89 vs 0.43, Mann-Whitney p = 0.032). There was no significant correlation between age and APP scores for either brain region.

Assessment of Olfactory Bulb Primary Sensory Afferents and Other Neuronal Constituents

As results from the gene expression comparison indicated several-fold greater numbers of DEGs in the OB as compared to AMY, this suggested a greater impact of COVID-19 on the OB. Unexpectedly, this was apparently not due to a higher rate, in the OB, of detected SARS-CoV-2 viral RNA sequences, as there were only 5 DEGs when comparing RT-PCR-positive and negative OB samples. The neuronal composition of the OB was therefore assessed with immunohistochemical stains for SNAP-25, a general marker of neuronal synapses, TH, a marker of a specific OB neuronal type, and OMP-1, a specific marker of afferent fibers originating from the nasopharyngeal olfactory sensory mucosa, as previously published in preprint form (141). Table 8 shows basic data for the cases and controls studied. COVID-19 cases did not significantly differ in any category from the non-COVID-19 cases. Supplementary Data Table S1 indicates the cases and controls that were used for each stain.

Figure 12 shows photomicrographs of OMP-1, TH and SNAP-25 immunoreactivity in COVID-19 and non-COVID-19 control cases. Positive OMP-1 staining was restricted to the peripheral nerve fiber and glomerular layers while TH and especially SNAP-25 were more diffusely distributed throughout the bulb. Qualitative examination of the OMP-1-stained sections indicated lighter staining of synaptic glomeruli in OB of COVID-19 cases as compared with controls (arrows in Fig. 12A, G).

Figure 13 shows comparisons of the area occupied by OMP-1, TH and SNAP-25 staining in OB of COVID-19 and control cases. The immunoreactive area occupied by OMP-1 staining was significantly reduced in COVID-19 cases, to about 60% of that in control cases (p = 0.006). Analysis of variance showed an overall difference in OMP-1 immunoreactivity between the groups when controls were subdivided by the presence or absence of non-COVID-19 pneumonia (p = 0.022); pairwise post hoc significance testing showed significant differences between the COVID-19 group and the controls without pneumonia (p = 0.048) but no differences between the COVID-19 group and the controls with pneumonia. There was no statistical difference between controls with and without pneumonia.

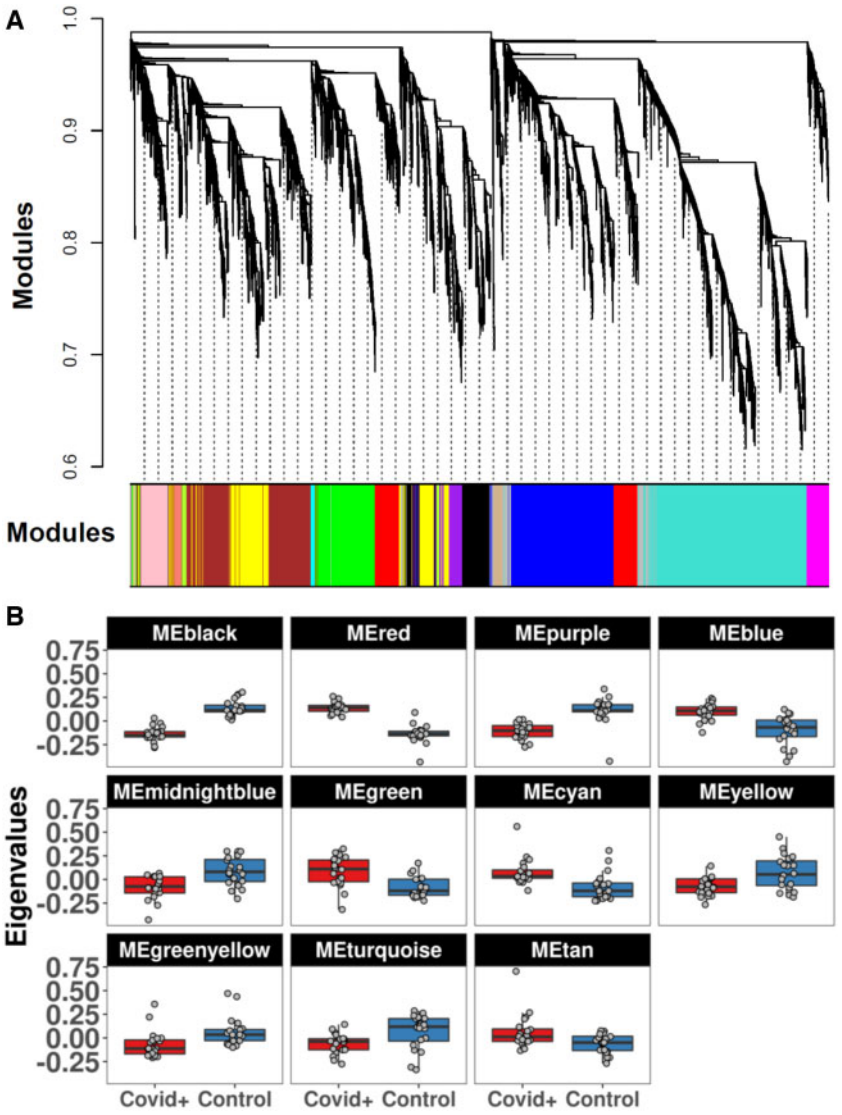

FIGURE 9. Dendrogram representing the relationship between WGCNA modules from OB.

Analysis of variance showed no significant group differences for TH while for SNAP-25 the group difference was significant ($p = 0.029$), with significantly less SNAP-25 staining in controls with pneumonia as compared to controls without pneumonia ($p = 0.025$) but no significant differences between COVID-19 cases and all controls, or between COVID-19 cases and controls subdivided by presence or absence of pneumonia.

As COVID-19 cases differed with respect to the presence or absence of OB SARS-CoV-2 RNA sequences, we also compared immunoreactivity for the 3 proteins in the PCR-positive and PCR-negative COVID-19 cases versus all controls. For OMP-1, analysis of variance showed a significant difference between groups ($p = 0.02$); post hoc testing showed a significant difference between OBT-PCR-negative COVID-19 cases and controls ($p = 0.027$) but no significant difference between OBT-PCR-positive cases and controls ($p = 0.344$). Analysis of variance of the same groups for TH or SNAP-25 staining showed no significant group differences ($p = 0.239$ and 0.714, respectively).

Microglial Assessment in Olfactory Bulb, Amygdala and Cerebellar Cortex

As results from the gene expression comparison indicated enrichment of immune pathways, including interferon signaling and the toll like receptor cascade, and as microglia are the primary immune effector cells in the brain, the area fraction of brain regions occupied by Iba1, a pan-microglial marker, and by LN3, a marker of HLA-DR and hence microglial activation, were immunohistochemically assessed. Ta-

TABLE 7. Summary of the WGCNA Analysis in OB, Including the Number of Genes, Differential Analysis Between COVID-19 Cases and Controls, Enrichment of Pathways and Cell-Specific Genes, and Hub Genes for Each Co-Expression Network

Module	Genes (n)	Direction COVID-19 vs CTL	Adj-p	Cell	Pathways	Hub Gene
Black	459	DOWN	1.7E−11	–	Ribosome/RNA metabolism	*CLSTN1*
Red	587	UP	1.7E−11	–	Cilium/Taste	*DMTF1*
Purple	223	DOWN	3.5E−06	–	Mitochondrion	*PJA2*
Blue	1248	UP	3.4E−05	–	–	*ZNF767P*
Green	726	UP	6.5E−04	End, Per	Development, Angiogenesis	*COL1A2*
Mid. blue	39	DOWN	6.5E−04	Ast	–	*ENHO*
Cyan	59	UP	2.0E−03	–	–	*BTBD19*
Yellow	848	DOWN	3.1E−03	Ast, Oli	Vesicles	*NEBL*
Grn/yell	105	DOWN	1.0E−02	Ex, In	Synaptic signaling	*CNR1*
Turquoise	1904	DOWN	1.2E−02	Ex, In	Synaptic signaling	*CAMK2B*
Tan	103	UP	1.5E−02	–	Interferon/Immune	*PARP9*
Magenta	244	–	0.134	–	–	*LOC100996573*
Salmon	87	–	0.153	–	Protein folding	*DNAJB1*
Brown	1043	–	0.210	Oli, Ast, Per	Development, Cytoskeleton	*SORBS1*
Pink	314	–	0.210	Mic	Immune	*NCKAP1L*

ble 9 shows basic data for the cases and controls studied. Due to less remaining OB tissue for Mayo Clinic cases, these were not included. Other than for age in the AMY and cerebellum (CBL) subsets, COVID-19 cases did not significantly differ in any category from the non-COVID-19 cases.

Figure 14 shows representative photomicrographs of staining for Iba1 in COVID-19 and control cases in AMY, CBL, and OB, and Figure 15 shows results of the quantification of the area occupied by the staining. The area occupied by Iba1-immunoreactive microglia was significantly reduced in AMY and CBL of COVID-19 subjects. The control group did not differ with presence or absence of pneumonia and so these were combined into a single control category for the graphs. The area of OB occupied by Iba1-stained microglia did not differ between COVID-19 and control cases.

The area occupied by LN3-immunoreactive microglia did not differ between cases and controls, in AMY, CBL, and OB, whether or not controls were subdivided by presence or absence of non-COVID-19 pneumonia (results not shown).

Cytokine and Protein Arrays in Amygdala, Blood Serum, and CSF

The results for gene expression in OB and AMY were suggestive of alterations in inflammation or immune-related proteins, and prior reports have generally agreed that there are elevated levels of circulating cytokines in subjects with COVID-19. Therefore, we wished to directly assess the concentrations of a set of cytokines in AMY, as well as in postmortem blood serum, in a subset of subjects using a commercial multiplex antibody array (RayBiotech, Inc.; see Materials and Methods). Table 10 shows basic data for the cases and controls studied. COVID-19 cases from which AMY samples were analyzed were significantly younger than the comparison control group, but otherwise, cases and controls did not significantly differ in any category.

Results for the AMY samples showed significant differences between groups in 7 of the 20 measured cytokines, all with decreased concentrations in the COVID-19 samples (Fig. 16). AMY cytokine concentrations in control cases with or without pneumonia did not differ significantly (results not shown). Only one cytokine comparison (MMP-9) was significant in serum samples (Fig. 17); however, all 5 comparisons with the lowest p values showed increased concentrations in the COVID-19 serum samples.

DISCUSSION

The causes of COVID-19 neurological effects (1–10) are unclear, as most studies (11–40) agree that SARS-CoV-2 brain invasion occurs in only a relatively small fraction of fatal COVID-19 cases, and when present, viral copy numbers are generally very low, perhaps representing only broken-down genomic fragments. The detection of subgenomic SARS-CoV-2 sequences has been suggested to prove that in situ viral replication has taken place, but even in COVID-19 lung or throat, only a subset of cases have had these (21, 157).

In our comprehensive survey (154) of 16 brain regions of 20 COVID-19 cases, SARS-CoV-2 RNA was detected in only 2.5% (7/320) of sampled brain regions, and in only 4 of 20 cases (20%). However, differing PCR protocols have differing sensitivity and specificity (16, 19, 40, 158–161) and therefore the true prevalence of viral brain entry may be difficult to establish. When we repeated our RT-PCR screening on OB, AMY and ENT with additional primers and probes for the E, N1, N2, RdRp, and S genes, we found more cases with

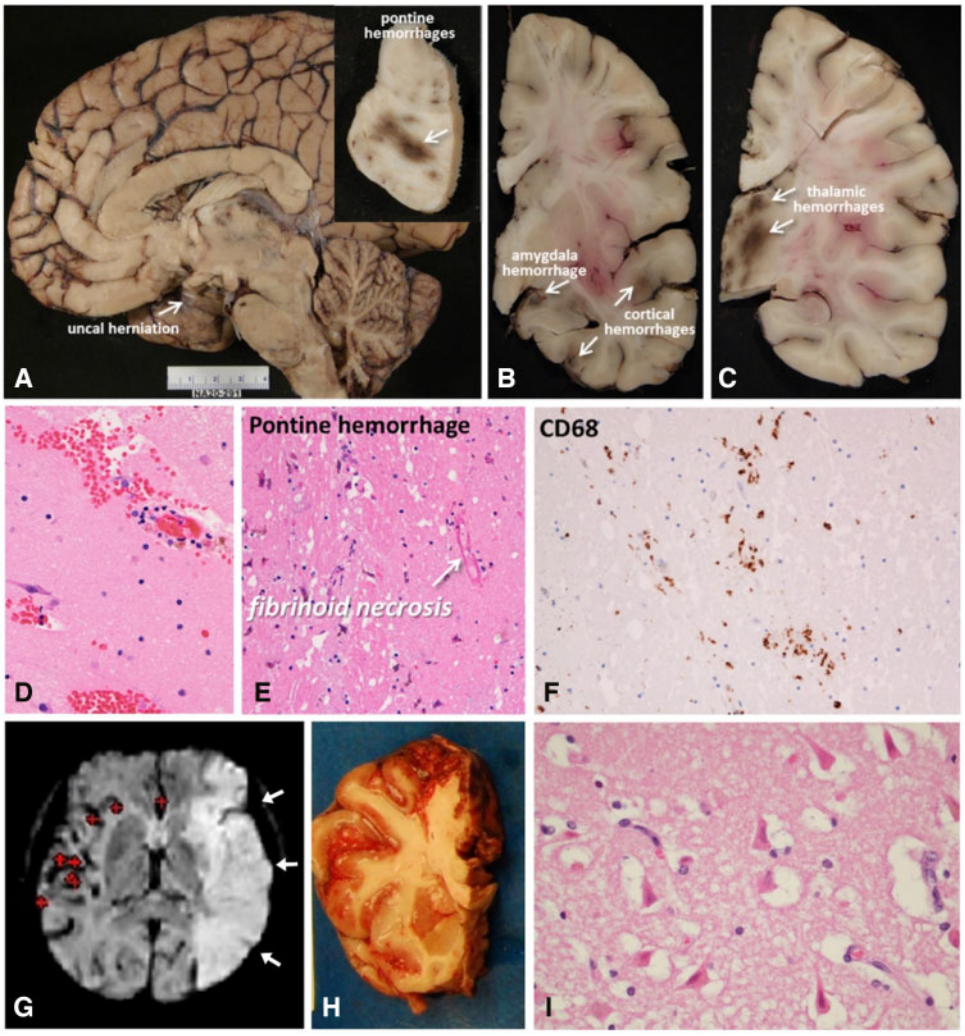

FIGURE 10. (A-F) Mayo Clinic COVID-19 case 10, a 38-year-old man. Neuropathological gross examination was consistent with brain swelling causing transtentorial uncal herniation and acute hemorrhages (arrows **A** and **A** inset, **B** and **C**). Microscopic hemorrhage was present in temporal lobe (D), with fibrinoid vascular necrosis in the pons **(E)** and neuropil infiltration with CD-68-immunoreactive macrophages **(F)**. **(G-I)** Banner Sun Health Research Institute (BSHRI) COVID-19 case, a 74-year-old man. Clinical findings indicated a massive acute left middle cerebral artery territory ischemic infarct, as shown in the MRI image (**G**, white arrows). Gross examination of the brain at autopsy showed hemorrhage within the cerebral cortex **(H)**. Widespread areas within the left middle cerebral artery distribution showed acute ischemic infarction and/or acute hypoxic-ischemic changes, with perikaryal cytoplasmic eosinophilia and nuclear pyknosis of cortical pyramidal neurons **(I)**.

Ct 40 or lower in OB, for a total of 8/21 (38%), but no additional new positive regions.

We found only 2/42 cases (4.8%) that had major postmortem findings that were likely to have been attributable to their terminal COVID-19 illness (154). Only one of these was histopathologically typical of viral infection, with acute encephalitis and neuropil infiltration by lymphocytes and macrophages, as well as being RT-PCR-positive for SARS-CoV-2 in an affected area. Herpes encephalitis was considered but thought less likely due to the lack of the characteristic intranuclear inclusions. As histological findings consistent with viral encephalitis are rare in routine autopsies, and as viral RNA was present, we think that this may be one of the very few cases of encephalitis due to SARS-CoV-2.

The other case had a large acute middle cerebral artery territory ischemic and hemorrhagic infarction several days after the clinical onset of his COVID-19 disease, accompanied by bilateral lower extremity arterial thromboses; no brain region from this case had SARS-CoV-2 RNA detected. Although it is difficult to attribute observed pathology, in any single autopsy, to COVID-19 as opposed to non-specific agonal processes, such widespread thromboses were reportedly common autopsy findings early in the pandemic (15, 20, 30, 90). The quick standardized adoption of prophylactic subcutaneous low-dose heparin may have been effective in minimizing these, but in this subject in our study, it is possible that it was administered too late in his illness.

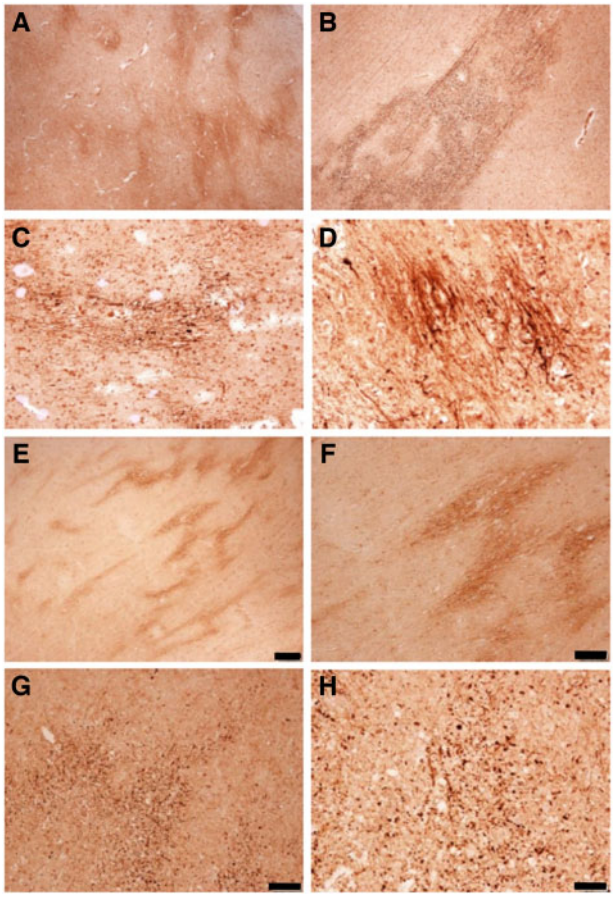

FIGURE 11. Photomicrographs of cingulate gyrus and precentral white matter APP staining in COVID-19 cases **(A-D)** and controls **(E-H)**. **(A)** Low-magnification, cingulate gyrus, COVID-19 case. **(B)** Low-magnification, precentral gyrus, COVID-19 case. **(C)** Medium-magnification, precentral gyrus, COVID-19 case. **(D)** High-magnification, cingulate gyrus, COVID-19 case. **(E)** Low-magnification, cingulate gyrus, control case, with non-COVID-19 pneumonia. **(F)** Low-magnification, precentral gyrus, control case, with non-COVID-19 pneumonia. **(G)** Medium-magnification, precentral gyrus, control case, with non-COVID-19 pneumonia. **(H)** High-magnification, cingulate gyrus, control case, with non-COVID-19 pneumonia. Bar in E also serves for A = 200 mm. Bar in F also serves for B = 100 mm. Bar in G also serves for C = 50 mm. Bar in H also serves for D = 50 mm.

Acute or subacute infarctions and/or acute hypoxic-ischemic microscopic changes were not significantly more common in 42 COVID-19 cases than in 107 controls (9.5% vs 10.3% for controls), nor were acute hemorrhages or microhemorrhages (9.5% vs 2.8%). Staining for APP, a presumptive marker of agonal hypoxia-ischemia and reported in COVID-19 cases (54, 55), was not more common in COVID-19 cases than in controls (156) but had significantly higher density scores when compared with controls, although not in comparison to controls with non-COVID-19 pneumonia.

Microvascular, acute and subacute ischemic, and/or hemorrhagic lesions (4, 11, 13, 20, 26, 30, 33, 35, 36, 38, 39, 45–50, 53–62) have frequently been reported in COVID-19 but these are also common in unselected autopsy series. We found that acute and subacute ischemia, infarction, and hemorrhage were present in the brains of up to 14% of 691 consecutive pre-COVID-19 autopsies with or without concurrent autopsy-proven pneumonia (162). In comparison, in reviews of COVID-19 publications, reported clinically determined rates of acute brain infarction or hemorrhage range from 0.5% to 20% (1, 4, 5, 13, 25, 26, 28, 29, 32, 34–36, 38, 39, 45–48, 53–55, 156, 163–175). Variability between COVID-19 reports may be at least partially due to the delayed introduction of anti-coagulant agents as standard COVID-19 therapy (176, 177).

No intracytoplasmic or intranuclear viral inclusions were seen in any of the cases, including the COVID-19 case with acute encephalitis. Microglial nodules were rare, limited to 2 COVID-19 cases without local SARS-CoV-2 detected. Significant perivascular cuffing with mononuclear cells was only seen in the Mayo Clinic encephalitis case. Perivascular demyelination suggestive of ADEM was not seen in any case or control. The lack of specific viral histopathology in COVID-19 brains has had generally wide agreement in the literature (12–16, 18, 19, 25, 26, 28, 29, 32–34, 36, 40, 46–55, 113, 163, 178).

Overall, we detected numerous gene expression changes in both OB and AMY from COVID-19 cases, but with approximately 7-fold greater numbers of DEGs in OB. No co-expression network differences were detected in AMY whereas we detected 11 modules with significant changes in OB; these may suggest possible critical pathogenic processes and therapeutic targets. At the pathway level, we detected some commonalities between regions, including the downregulation of synaptic genes and upregulation of some immune system genes, but also some differences found only in OB, including enrichment of olfactory/taste receptor genes. The hub gene in the co-expression network enriched for taste receptors and signaling was *DMTF1* (cyclin D binding Myb-like transcription factor 1), encoding for a transcription factor induced by the oncogenic Ras signaling pathways and functioning as a tumor suppressor.

Neuroinflammation has been widely reported in COVID-19 disease (62, 179, 180) but relatively few reports characterize this in detail and broad confirmation is lacking. The hub gene detected in the immune module was *PARP9* (poly(ADP-ribose) polymerase family member 9) which is involved in interferon-mediated antiviral defense (181, 182). It has been recently demonstrated that the ectopically expressed SARS-CoV-2 Nsp3 macrodomain hydrolyzes PARP9/DTX3L-dependent ADP-ribosylation induced by IFN signaling, suggesting a role for this modification as a putative effector of the IFN response (183). Also, previous reports demonstrated an induction of interferon signaling genes and IFNγ-induced STAT1 phosphorylation (181, 182).

We detected a dysregulation of synaptic and neuronal genes in both OB and AMY, as demonstrated by pathways and WGCNA analysis. Some of the relevant genes were the hubs of the 2 distinct WGCNA co-expression networks involved in OB, enriched for synaptic and neuronal processes as well as for both excitatory and inhibitory neuronal genes. *CNR1* (cannabinoid receptor 1 [CB1]) is the hub of the green-

TABLE 8. Demographic, Pneumonia, and Neuropathological Characteristics of COVID-19 and Control Cases Used for Olfactory Bulb Neuronal Assessment

Group	Age Median (Range)	Female N (%)	Acute Lung Injury or Acute Pneumonia N (%)	ApoE-ε4 n (%)	Major Neuropath Dx n (%)	Braak Neurofibrillary Stage Median (Range)	Thal Amyloid Phase Median (Range)
COVID-19 n = 18	81 (67–93)	7/18 (39%)	14/15 (93%)	5/18 (28%)	10/18 (56%)	4 (1–6)	3.5 (0–5)
Control n = 28*	87 (71–103)	10/28 (36%)	15/28 (54%)	7/27 (26%)	15/27 (55%)	4 (2–6)	3 (0–5)

*For control group N, OMP-1 = 27, TH = 22; SNAP-25 = 23.
See Table 3 for explanation of column titles and Table 1 for listing of cases used for each OB neuronal marker.

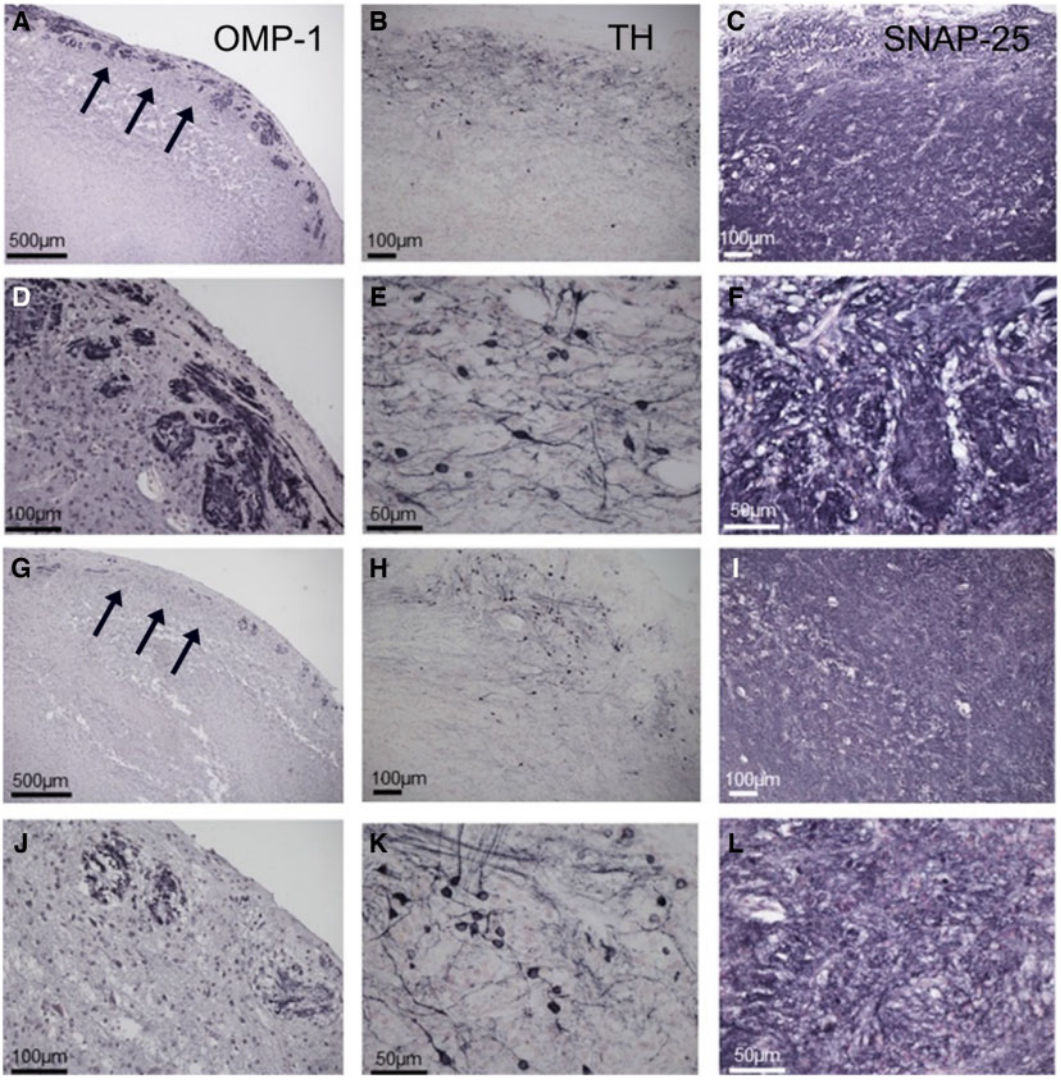

FIGURE 12. Photomicrographs of representative OMP-1, TH, and SNAP-25 immunoreactivity in **(A-F)** non-COVID-19 control cases and **(G-L)** COVID-19 cases at low **(A-C, G-I)** and higher **(D-F, J-L)** magnifications. The higher magnifications were used for image analysis. Columns of images are, from left to right, portraying OMP-1, TH, and SNAP-25 staining of olfactory bulb. Note the loss and/or decreased staining of synaptic glomeruli (arrows) in COVID-19 olfactory bulb.

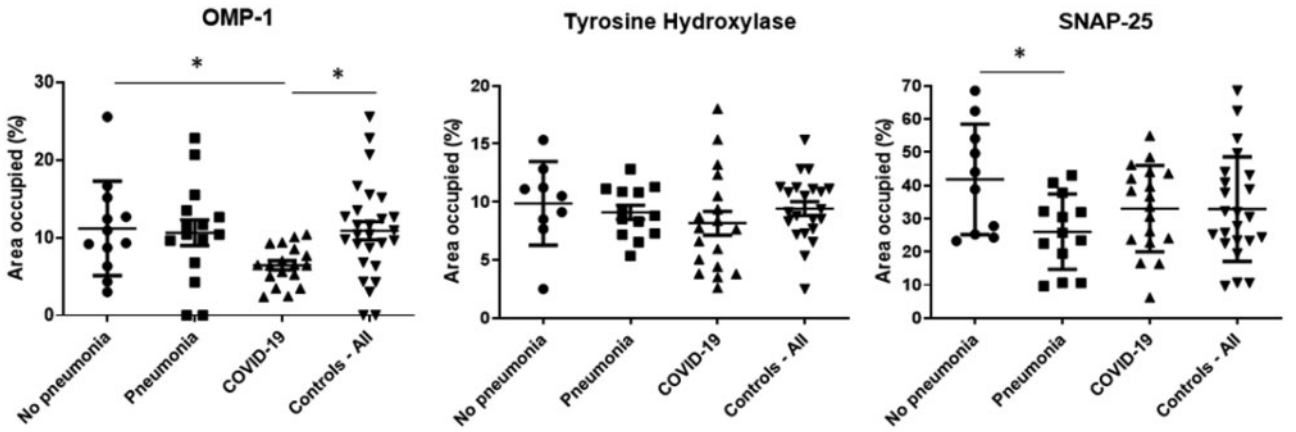

FIGURE 13. Quantification results for OMP-1, TH, and SNAP-25 immunoreactivity for each group. Shown are controls grouped together or separated by presence or absence of pneumonia. Means and standard deviations are shown. OMP-1 is significantly depleted in COVID-19 cases relative to all controls and relative to controls without pneumonia. SNAP-25 staining is significantly depleted in control subjects with pneumonia as compared to control subjects without pneumonia. *$p < 0.05$.

TABLE 9. Demographic, Pneumonia, and Neuropathological Characteristics of COVID-19 and Control Cases Used for Microglial Assessment

Group	Age Median (Range)	Female N (%)	Acute Lung Injury or Acute Pneumonia n (%)	ApoE-ε4 N (%)	Major Neuropath Dx n (%)	Braak Neurofibrillary Stage Median (Range)	Thal Amyloid Phase Median (Range)
Amygdala							
COVID-19 n = 29	78* (38–93)	15/29 (52%)	14/15 (93%)	5/20 (25%)	19/29 (65%)	4 (0–6)	3 (0–5)
Control n = 27	86 (71–103)	12/27 (44%)	15/27 (55.5%)	5/27 (18.5%)	17/27 (63%	4 (0–5)	3 (0–5)
Cerebellum							
COVID-19 n = 28	78.5* (38–93)	14/28 (50%)	14/15 (93%)	5/19 (26%)	18/28 (64%)	4 (0–5)	3 (0–5)
Control n = 30	86 (71–103)	13/30 (43%)	16/30 (53%	6/30 (20%)	17/30 (57%)	4 (2–6)	3 (0–5)
Olf. Bulb							
COVID-19 n = 18	81 (67–93)	7/18 (39%)	14/15 (93%)	5/18 (28%)	9/18 (50%)	4 (1–6)	3.5 (0–5)
Control n = 29	87 (71–103)	12/29 (41.3)	16/29 (55%)	6/29 (21%)	17/29 (59%)	4 (2–6	3 (0–5)

*Unpaired, 2-tailed t-test $p < 0.005$.
See Table 3 for explanation of column titles.

yellow module and mediates the biological activity of both endogenous and exogenous cannabinoids centered on psychoactive functions (184). There are multiple lines of evidence regarding the effects of cannabinoid receptors on viral infection. Activation of CB1 inhibits the production of proinflammatory mediators, such as NO or TNFα, and inhibits Ca2+ channels. On one hand, the activation of CB1 increases the progression of viral diseases through an immunosuppressive effect, but on the other hand it might inhibit the immune effects derived from the viral infection by eliciting an immunoprotective profile (184). In our study we see a dysregulation of the network regulated by CB1, and we hypothesize this might be a feedback effect aimed at reducing the neuroinflammatory state induced by the viral infection.

The hub gene of the turquoise module (n = 1904 genes) is *CAMK2B* (calcium/calmodulin dependent protein kinase II beta) and is involved in dendritic spine and synapse formation, and neuronal plasticity and development (185). *CAMK2B* mutations and mRNA alterations have been associated with neurodevelopmental diseases, epilepsy, intellectual disability, and schizophrenia (186–188). Cognitive and attention deficits, new-onset anxiety, depression, psychosis, and seizures have

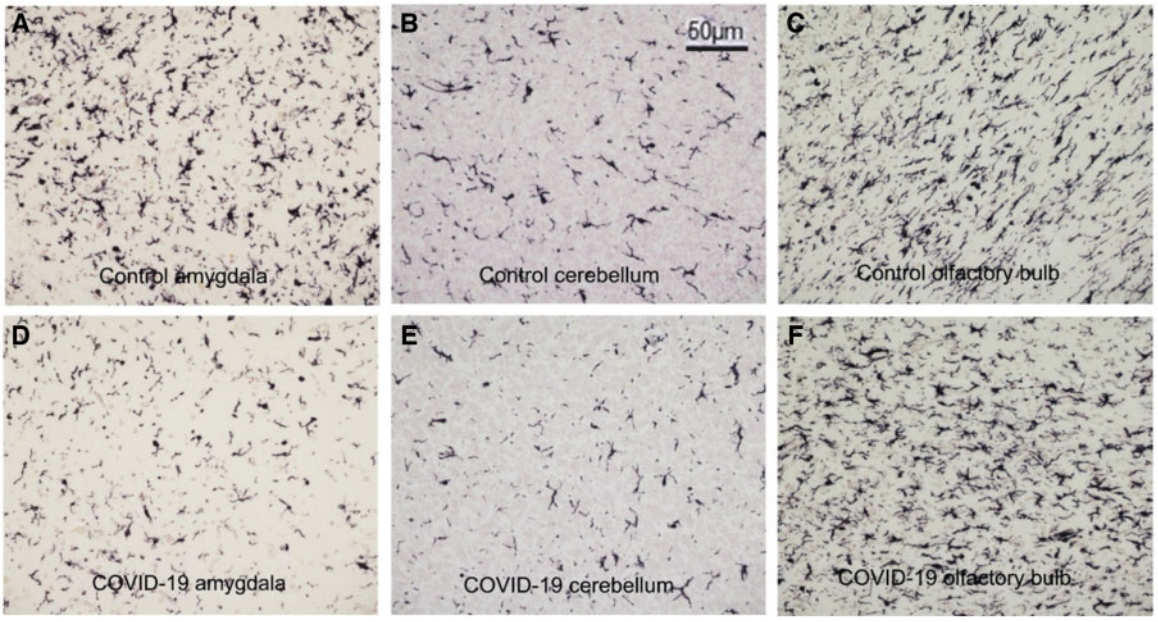

FIGURE 14. Photomicrographs of immunohistochemical Iba1 staining of microglia in control subjects **(A-C)** and COVID-19 cases **(D-F)**, in amygdala **(A, D)**, cerebellar cortex **(B, E)**, and olfactory bulb **(C, F)**. Scale bar in B serves for all frames.

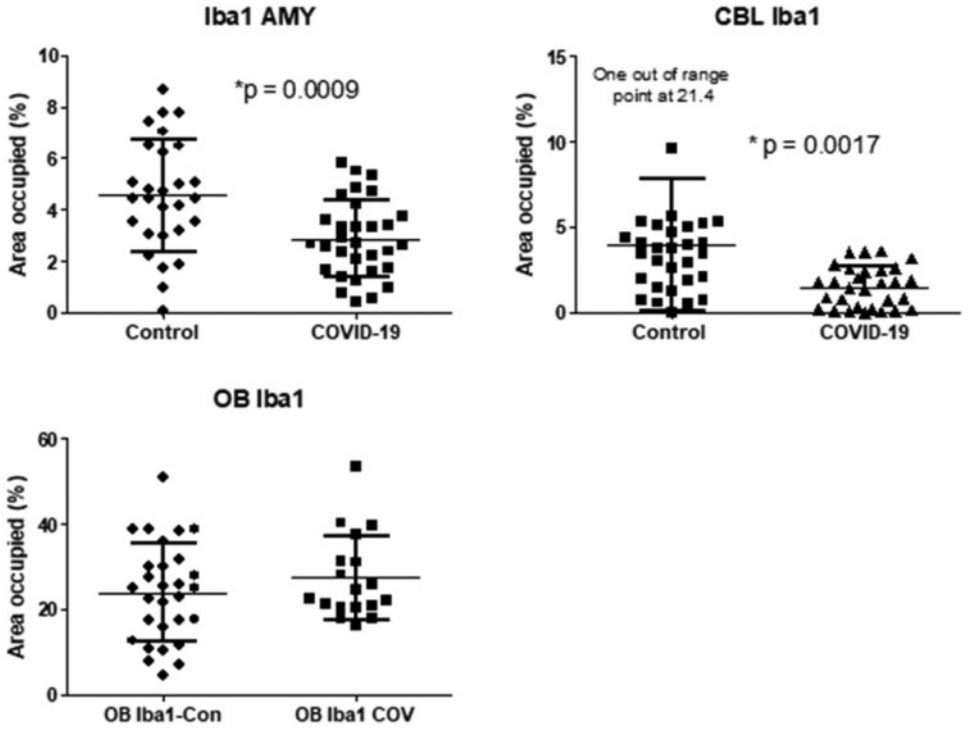

FIGURE 15. Quantification results for Iba1 staining of microglia in COVID-19 and control subjects. The control group did not differ with presence or absence of pneumonia and so these were combined for the graphs. The area occupied by Iba1-immunoreactive microglia is significantly reduced in AMY and CBL of COVID-19 subjects. Means and standard deviations are shown.

been observed in some patients with COVID-19, unrelated to respiratory insufficiency (189). These symptoms, as well as the dysregulation of the CAMK2B network synaptic genes, may be a consequence of circulating cytokine alterations induced by COVID-19 infection (190–192). CAMK2B might therefore be a promising target.

TABLE 10. Demographic, Pneumonia, and Neuropathological Characteristics of COVID-19 and Control Cases Used for Cytokine Array Analyses

Group	Age Median (Range)	Female n (%)	Acute Lung Injury or Acute Pneumonia N (%)	ApoE-ε4 n (%)	Major Neuropath Dx n (%)	Braak Neurofibrillary Stage Median (Range)	Thal Amyloid Phase Median (Range)
Serum							
COVID-19 n = 15	84 (73–96)	8/15 (53%)	9/12 (75%)	4/15 (27%)	10/15 (67%)	4 (2–6)	4 (0–5)
Control n = 7	83 (60–103)	2/7 (29%)	1/5 (20%)	3/7 (43%)	4/7 (57%)	5 (4–6)	3 (0–5)
Amygdala							
COVID-19 n = 26	78* (38–93)	12/26 (48%)	12/13 (92%)	5/17 (28%)	17/26 (63%)	4 (0–6)	4 (0–5)
Control n = 24	87.5 (71–100)	10/24 (42%)	15/24 (62.5%)	5/23 (22%)	14/24 (58%)	4 (2–6)	3 (0–5)

*Two-tailed, unpaired t-test p = 0.005.
See Table 3 for explanation of column titles.

One of the OB-specific processes we identified was angiogenesis/blood vessel development (WGCNA—green module, Fig. 9) with upregulation of these processes in COVID-19 patients. Also, there was enrichment of endothelial cell and pericyte specific genes in OB. The hub gene in the green module is *COL1A2 (*collagen type I alpha 2 chain), encoding for the α2 polypeptide of Type I collagen, a powerful angiogenesis inducer (193). SARS-CoV-2 has been hypothesized to enter brain endothelial cells activating neutrophils, macrophages, and thrombin production, promoting microthrombi deposition, capillary congestion and ischemic lesions and disturbing neurotransmitter synthesis (31, 194). Angiogenesis is a response against tissue damage and hypoxia, and in COVID-19 has been observed in different tissues, including the brain (195). *COL1A2* might potentially be a candidate therapeutic target to reverse/minimize the microvascular damages induced by COVID-19 neuroinflammation.

While both OB, and to a lesser extent, AMY, showed pronounced gene expression changes in COVID-19, the changes in OB were several-fold more numerous (5405 DEGs in OBT vs 728 in AMY). This difference, as well as our finding that OB is the most likely brain region to harbor SARS-CoV-2, strongly supports the OB as the most probable CNS entry site, in agreement with suggestions by prior studies (11, 36, 40, 63, 64, 196–200). Surprisingly, however, there were only 5 OB DEGs between COVID-19 cases with and without detected SARS-CoV-2 RNA sequences in OB. This remarkable finding, along with the widely documented hyposmia in many COVID-19 patients (64–66), led us to examine the olfactory mucosal afferents to OB. Immunohistochemical assessment of OMP-1, a specific marker of these afferents (201–203) that is severely depleted in animal model lesions of olfactory epithelium (204–208), revealed a 60% reduction in COVID-19 OB across both SARS-COV-2 RT-PCR-positive and -negative OBs. As spontaneous discharge of olfactory epithelial afferents dictates intra-OB neurophysiological activity and connectivity (208–210), it appears possible that deafferentation during COVID-19 is responsible for the majority of our observed OB transcriptional changes.

Resultant transsynaptic effects might be mediating many of the AMY gene expression changes. The AMY and other brain regions have monosynaptic connections with the OB. Olfactory stimulation activates neurons of the AMY (211), while olfactory bulbectomy in mice has been reported to cause piriform cortex reactions including activation of interneurons, apoptosis of pyramidal neurons and downregulation of regulatory pathways (212–216). Recent imaging studies (217–219) are consistent with COVID-19-related transsynaptic selective atrophy and/or gray matter changes of olfactory system brain structures, including OB, primary olfactory cortex, AMY, parahippocampal gyrus, and orbitofrontal cortex. Metabolic imaging with ^{18}F-FDG PET in patients with "long COVID" found hypometabolism in the AMY, hippocampus, and bilateral rectal and orbital gyri (220), similarly to the decreased cerebral glucose utilization reported after olfactory bulbectomy in an animal model (221).

Transsynaptic changes following olfactory deafferentation may have diverse behavioral effects. Olfactory bulbectomy is the basis of a rat model of depression (222–227) associated with inflammatory and intermediate early gene expression in the AMY, and olfactory bulbectomy has been associated with memory and cognitive deficits thought to be related to basal forebrain cholinergic and/or glutamatergic effects (228–232). As OB deafferentation in animal models, like hyposmia in COVID-19 subjects, is most often reversed within months of the initial lesion or infection, it seems doubtful, however, that transsynaptic effects and any associated neurological symptoms would persist over a longer term although this deserves investigation.

A surprising finding of our studies was the areal decrease in Iba1-labeled microglia in both AMY and CBL, with no change in LN3-labeled ("activated") microglia. Together with the reduction of several AMY cytokines, this suggests a significant COVID-19-associated immunosuppression of

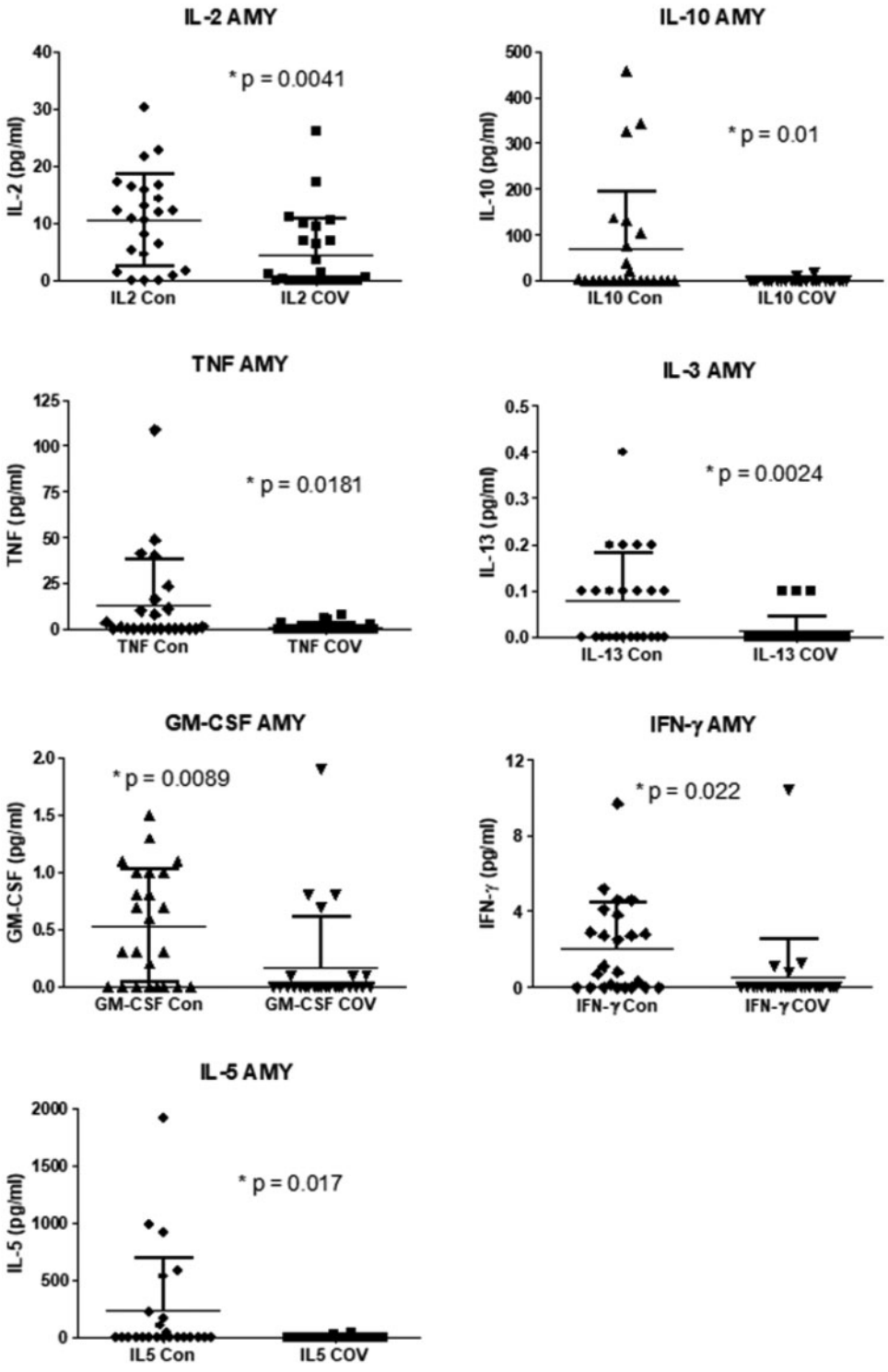

FIGURE 16. Scatter plots showing results for cytokines that showed significant group differences in amygdala samples. All 7 comparisons demonstrated decreased concentrations in COVID-19 cases relative to controls. The control group did not differ with presence or absence of pneumonia and so these were combined for the graphs. Means and standard deviations are shown.

brain immune effector cells. Although immunosuppression as a result of acute COVID-19 disease might seem unlikely, there have been reported indications of this, including reduced numbers, gene expression and morphological abnormalities of monocytes (233–236) as well as disrupted germinal centers and dendritic cell networks of lymph nodes (237–239); these

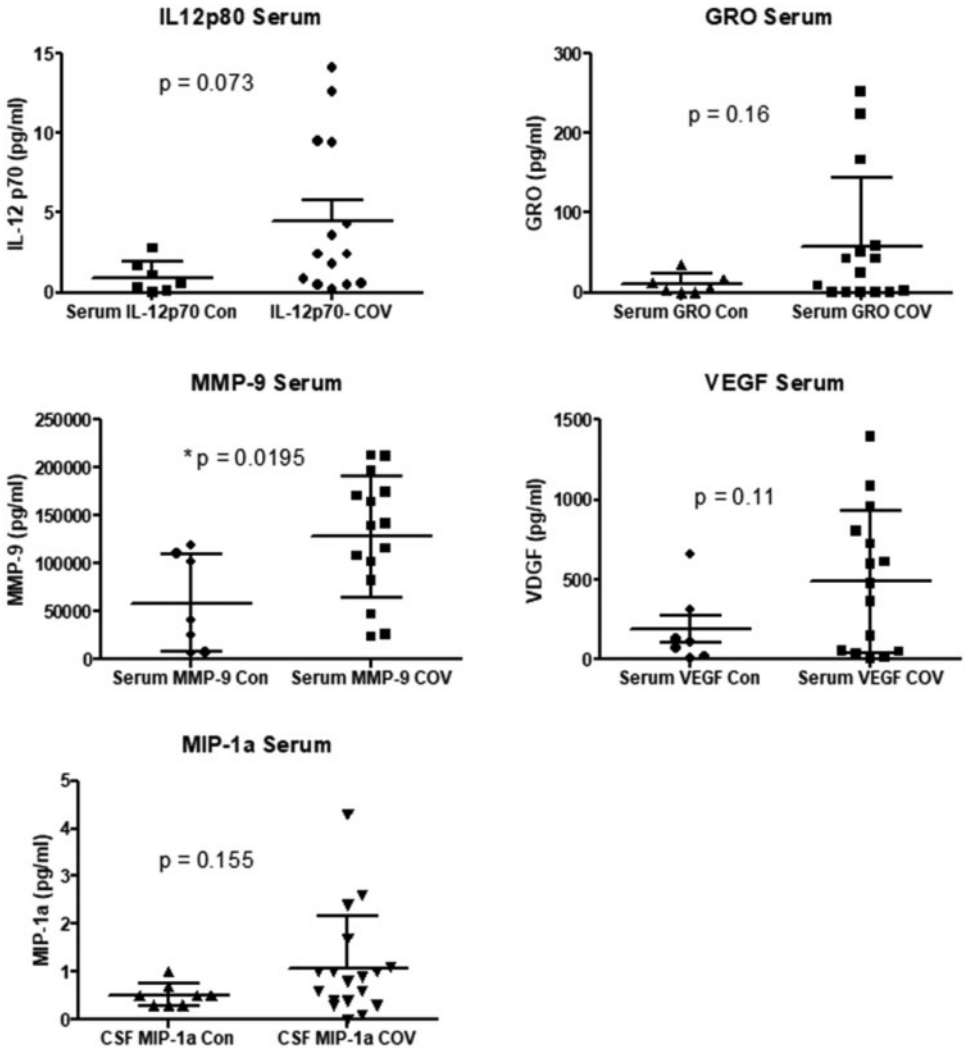

FIGURE 17. Scatter plots showing results for cytokines that showed group differences in postmortem serum samples. All 5 comparisons demonstrated increased concentrations in COVID-19 cases relative to controls, but only 1 of 5 comparisons reached the significance level. The control group did not differ with presence or absence of pneumonia and so these were combined for the graphs. Means and standard deviations are shown.

cell types are homologues of microglia. An "exhaustion-like" NK-cell phenotype has been described in COVID-19 (240) that may be related to persistent exposure to inflammatory signals such as IL-15, and may be analogous to the "dystrophic" microglia seen in a variety of CNS pathologies (241–245). We did not find a significant change in Iba1 staining in OB, perhaps due to the additional, deafferentation-induced, microglial stimulus that was not present in CBL or AMY.

There are considerable interindividual differences in the COVID-19 circulating immune profile, as well as changes during the clinical course, with some evidence of an early immunosuppressive or maladapted immune response (233–236, 240, 246). Early lymphopenia, including decreases in circulating CD4 and CD8 cells, is relatively common. While the attention has been on "cytokine storm" in acute COVID-19, this may be an oversimplification. For example, elevations in IL-6 have been identified not only in acute COVID-19 but also in other critical illnesses such as sepsis and acute respiratory distress syndrome, and while the pro-inflammatory effects of IL-6 are well known, it may also play an anti-inflammatory role. Complicating such scenarios is the likelihood that the circulating cytokine profile evolves differently between subjects and day-to-day in the initial days and weeks of the acute illness (246, 247). Generally, however, the immune response triggered by COVID-19 infection results in an increase of serum cytokines including IL-1, IL-6, IL-10, and TNF-α (248, 249) and this is paralleled to some extent in our finding of elevations of 4 cytokines, IL12p80, GRO, VEGF, MIP-1a, and MMP-9, in postmortem COVID-19 blood serum.

An important issue is whether or not COVID-19 lower respiratory disease elicits more intense systemic repercussions than typical acute pneumonia. Our investigations (112, 156, 162) indicate that acute or subacute ischemic changes, infarctions or hemorrhages are probably not more common in

COVID-19 than they are in subjects dying without COVID-19 or with or without non-COVID-19 acute pneumonia. Early adoption of low molecular weight heparin therapy may have reduced thromboembolism in our study subjects, in comparison with COVID-19 decedents in the first few months of the pandemic. Pronounced differential gene expression in both AMY and OB was present when comparing COVID-19 and controls but there were only 2 and 1 DEGs in these regions when comparing controls with and without pneumonia. Staining for APP, a marker of acute or subacute white matter axonal damage, was significantly more intense in COVID-19 subjects when compared with all controls but not when compared with controls with non-COVID-19 pneumonia. In the OB, the significant difference in OMP-1 staining seen when comparing COVID-19 cases with all controls was no longer significant when the comparison group was limited to controls with pneumonia; there was no statistical difference between controls with and without pneumonia. Staining for TH was not significantly different between groups but SNAP-25 staining, while not differing between COVID-19 cases and controls, was significantly less in controls with pneumonia as compared to controls without pneumonia. Altogether, these mixed results suggest that COVID-19 has greater but similar effects on the brain as compared with common end-of-life acute pneumonia. A shortcoming of this aspect of our study is the lack of identification of the responsible pathogens in our non-COVID-19 pneumonia subjects. This is a common limitation to pneumonia studies (250). When pathogens are identified, they are viral more often than bacterial, with the top 3 in US hospitalized patients being human rhinovirus, influenza A and B, and Streptococcus pneumoniae (251). We did not attempt to determine, from clinical records or postmortem culture, the presence of associated pathogens, but the confluent intra-alveolar accumulation of neutrophils is generally regarded as indicative of a bacterial cause (252) and therefore our non-COVID-19 pneumonia group is likely to have been biased toward the inclusion of bacterial pneumonia and against the inclusion of purely viral pneumonia, although mixed bacterial and viral causes were very likely to have been common.

Although COVID-19 has reportedly caused disproportionate mortality in those with dementia (114), and the apolipoprotein E-ε4 allele, a genetic risk factor for Alzheimer AD, may be more common in subjects with severe COVID-19 disease (113, 115–119), in the set of subjects that we examined in these studies, there was no apparent predilection of COVID-19 for AD or other major aging-associated neuropathological diagnoses, or an association with the apolipoprotein E-ε4 allele. This may be due to insufficient subject numbers and statistical power, as in a much larger set of AZSAND subjects, we have reported that autopsy-confirmed acute pneumonia is significantly more common in those with concurrent neuropathologically diagnosed major neurodegenerative conditions (112). It is acknowledged, however, that all of these studies have not considered whether it is specific neurodegenerative processes or just being institutionalized, critically ill and bedbound that is linked to the increased COVID-19 and pneumonia risk.

There are definite limitations to our study. We did not have detailed clinical records for many subjects, due to their dying outside of a hospital. Also, as most subjects were in respiratory failure, it was difficult for clinicians to test olfaction or cognition. Very few subjects were Hispanic and none were non-Caucasian/white. More critically, in any study of COVID-19 in the brains of elderly subjects, the diversity of co-existing pathology will make it difficult to separate out the findings that may be definitely due to the infection as opposed to brain aging, AD, other neurodegenerative and cerebrovascular lesions, non-COVID-19 pneumonia or common agonal changes. However, these complications will cloud any study of COVID-19 neurological effects, and autopsy with full neuropathological examination, and preferably whole-body autopsy, offers the only chance to sort these out and discern what may be specifically due to SARS-CoV-2. While we here report on more COVID-19 and control autopsies than has been done in any previous study to date, our findings constitute only an initial, preliminary and tentative sketch of the possible brain effects of the COVID-19 pandemic. We have here endeavored, through comparison of subject subsets matched for likely confounders, to isolate SARS-CoV-2-related findings. To guard against misleading conclusions due to these selective group comparisons, we have included a comparison of unselected autopsies from a single center. Many more autopsies will be needed, however, to definitively separate SARS-CoV-2 effects from the complexity of concurrent chronic and agonal changes, especially in the elderly.

The possibility that COVID-19 might somehow increase risk for developing AD or other neurodegenerative diseases, years or even decades after the acute infection, must be considered. A surge of post-encephalitic parkinsonism in the first half of the last century is still potentially linked to the 1918-1919 global H1N1 influenza pandemic (126, 253), and Herpes virus (254) and other infectious agents (125) are still being considered as potential pathogenic factors for AD. Coronaviruses have proven neurotropic potential, based on extensive animal model and human data (255). Two human coronaviruses, strains 229E and OC43, have been detected by RT-PCR, Northern hybridization and in situ hybridization in 44% and 23%, respectively, of 90 human brains obtained from multiple brain banks throughout Europe, the UK and USA (256). Only prolonged follow-up studies of COVID-19 survivors will determine whether there is viral brain persistence and/or long-term neurological consequences.

Summary Points

- Results confirm that OB is the most probable site of viral CNS entry.
- OB deafferentation during acute/subacute infection is likely to be responsible for the majority of observed OB transcriptional changes.
- Typical histological changes of CNS viral infection, including microglial nodules and perivascular lymphocytes, are rare.
- Reduction of microglial area fraction in cerebellar cortex and AMY, coupled with cytokine array results, suggest net immunosuppressive effects on brain tissues.
- Acute and subacute ischemic changes, infarctions, or hemorrhages are not more common in COVID-19 patients than con-

trols, although this may be due to the widespread introduction of prophylactic heparin early in the pandemic.
- Staining for APP as a marker of acute/subacute white matter axonal damage was more intense in COVID-19 brains overall but not when compared with controls with non-COVID-19 pneumonia.

ACKNOWLEDGMENTS

We are all humbled by the volunteer individuals and their families who have selflessly consented to autopsy, allowing us to begin to understand the neurological consequences of COVID-19. Biospecimens from the Banner Sun Health Research Institute Brain and Body Donation Program, including those presented in this report, are available to qualified researchers upon request from https://www.brainandbodydonationregistration.org/.

REFERENCES

1. Yassin A, Nawaiseh M, Shaban A, et al. Neurological manifestations and complications of coronavirus disease 2019 (COVID-19): A systematic review and meta-analysis. BMC Neurol 2021;21:138
2. Varatharaj A, Thomas N, Ellul MA, et al.; CoroNerve Study Group. Neurological and neuropsychiatric complications of COVID-19 in 153 patients: A UK-wide surveillance study. Lancet Psychiatry 2020;7: 875–882
3. Delamarre L, Gollion C, Grouteau G, et al.; NeuroICU Research Group. COVID-19-associated acute necrotising encephalopathy successfully treated with steroids and polyvalent immunoglobulin with unusual IgG targeting the cerebral fibre network. J Neurol Neurosurg Psychiatry 2020;91:1004–6
4. Ghannam M, Alshaer Q, Al-Chalabi M, et al. Neurological involvement of coronavirus disease 2019: A systematic review. J Neurol 2020;267: 3135–53
5. Anand PZ, Zhou L, Hamer DH, et al. Neurologic findings among inpatients with COVID-19 at a safety-net U.S. hospital. Neurol Clin Pract 2021;11:e83–91
6. Kremer S, Lersy F, de Sèze SJ, et al.; For the SFNR-COVID Group. Brain MRI findings in severe COVID-19: A retrospective observational study. Radiology 2020;297:E242–51
7. Pons-Escoda A, Naval-Baudin P, Majos C, et al. Neurologic involvement in COVID-19: Cause or coincidence? A neuroimaging perspective. AJNR Am J Neuroradiol 2020;41:1365–9
8. Romero-Sanchez CM, Diaz-Maroto I, Fernandez-Diaz E, et al. Neurologic manifestations in hospitalized patients with COVID-19: The ALBACOVID registry. Neurology 2020;95:e1060–70
9. Ellul MA, Benjamin L, Singh B, et al. Neurological associations of COVID-19. Lancet Neurol 2020;19:767–83
10. Guerrero JI, Barragan LA, Martinez JD, et al. Central and peripheral nervous system involvement by COVID-19: A systematic review of the pathophysiology, clinical manifestations, neuropathology, neuroimaging, electrophysiology, and cerebrospinal fluid findings. BMC Infect Dis 2021;21:515
11. Xydakis MS, Albers MW, Holbrook EH, et al. Post-viral effects of COVID-19 in the olfactory system and their implications. Lancet Neurol 2021;20:753–61
12. Poloni TE, Medici V, Moretti M, et al. COVID-19-related neuropathology and microglial activation in elderly with and without dementia. Brain Pathol 2021;31:e12997
13. Lee MH, Perl DP, Nair G, et al. Microvascular injury in the brains of patients with Covid-19. N Engl J Med 2021;384:481–3
14. Klein R, Soung A, Sissoko C, et al. COVID-19 induces neuroinflammation and loss of hippocampal neurogenesis. Res Sq 2021;doi: 10.21203/rs.3.rs-1031824/v1
15. Hanley B, Naresh KN, Roufosse C, et al. Histopathological findings and viral tropism in UK patients with severe fatal COVID-19: A postmortem study. Lancet Microbe 2020;1:e245–53
16. Gagliardi S, Poloni ET, Pandini C, et al. Detection of SARS-CoV-2 genome and whole transcriptome sequencing in frontal cortex of COVID-19 patients. Brain Behav Immun 2021;97:13–21
17. Fullard JF, Lee HC, Voloudakis G, et al. Single-nucleus transcriptome analysis of human brain immune response in patients with severe COVID-19. Genome Med 2021;13:118
18. Cosentino G, Todisco M, Hota N, et al. Neuropathological findings from COVID-19 patients with neurological symptoms argue against a direct brain invasion of SARS-CoV-2: A critical systematic review. Eur J Neurol 2021;28:3856–65
19. Chertow C, Stein S, Ramelli S, et al. SARS-CoV-2 infection and persistence throughout the human body and brain. Res Sq 2021; doi: 10.21203/rs.3.rs-1139035/v1
20. Thakur KT, Miller EH, Glendinning MD, et al. COVID-19 neuropathology at Columbia University Irving Medical Center/New York Presbyterian Hospital. Brain 2021;144:2696–708
21. Bhatnagar J, Gary J, Reagan-Steiner S, et al. Evidence of severe acute respiratory syndrome Coronavirus 2 replication and tropism in the lungs, airways, and vascular endothelium of patients with fatal Coronavirus Disease 2019: An autopsy case series. J Infect Dis 2021;223: 752–64
22. Roden AC, Vrana JA, Koepplin JW, et al. Comparison of in situ hybridization, immunohistochemistry, and reverse transcription-droplet digital polymerase chain reaction for severe acute respiratory syndrome Coronavirus 2 (SARS-CoV-2) testing in tissue. Arch Pathol Lab Med 2021; 145:785–96
23. Sablone S, Solarino B, Ferorelli D, et al. Post-mortem persistence of SARS-CoV-2: A preliminary study. Forensic Sci Med Pathol 2021;17: 403–10
24. Skok K, Stelzl E, Trauner M, et al. Post-mortem viral dynamics and tropism in COVID-19 patients in correlation with organ damage. Virchows Arch 2021;478:343–53
25. Deinhardt-Emmer S, Wittschieber D, Sanft J, et al. Early postmortem mapping of SARS-CoV-2 RNA in patients with COVID-19 and the correlation to tissue damage. Elife 2021;10:e60631
26. Bihlmaier K, Coras R, Willam C, et al. Disseminated multifocal intracerebral bleeding events in three Coronavirus Disease 2019 patients on extracorporeal membrane oxygenation as rescue therapy. Crit Care Explor 2020;2:e0218
27. Freij BJ, Gebara BM, Tariq R, et al. Fatal central nervous system coinfection with SARS-CoV-2 and tuberculosis in a healthy child. BMC Pediatr 2020;20:429
28. Matschke J, Lutgehetmann M, Hagel C, et al. Neuropathology of patients with COVID-19 in Germany: A post-mortem case series. Lancet Neurol 2020;19:919–29
29. Deigendesch N, Sironi L, Kutza M, et al. Correlates of critical illness-related encephalopathy predominate postmortem COVID-19 neuropathology. Acta Neuropathol 2020;140:583–6
30. Wichmann D, Sperhake JP, Lutgehetmann M, et al. Autopsy findings and venous thromboembolism in patients with COVID-19: A prospective cohort study. Ann Intern Med 2020;173:268–77
31. Paniz-Mondolfi A, Bryce C, Grimes Z, et al. Central nervous system involvement by severe acute respiratory syndrome coronavirus-2 (SARS-CoV-2). J Med Virol 2020;92:699–702
32. Menter T, Haslbauer JD, Nienhold R, et al. Postmortem examination of COVID-19 patients reveals diffuse alveolar damage with severe capillary congestion and variegated findings in lungs and other organs suggesting vascular dysfunction. Histopathology 2020;77: 198–209
33. Al-Sarraj S, Troakes C, Hanley B, et al. Invited Review: The spectrum of neuropathology in COVID-19. Neuropathol Appl Neurobiol 2021; 47:3–16
34. Jensen MP, Le Quesne J, Officer-Jones L, et al. Neuropathological findings in two patients with fatal COVID-19. Neuropathol Appl Neurobiol 2021;47:17–25
35. Kantonen J, Mahzabin S, Mayranpaa MI, et al. Neuropathologic features of four autopsied COVID-19 patients. Brain Pathol 2020;30:1012–16
36. Meinhardt J, Radke J, Dittmayer C, et al. Olfactory transmucosal SARS-CoV-2 invasion as a port of central nervous system entry in individuals with COVID-19. Nat Neurosci 2021;24:168–75
37. Puelles VG, Lutgehetmann M, Lindenmeyer MT, et al. Multiorgan and renal tropism of SARS-CoV-2. N Engl J Med 2020;383:590–2

38. Remmelink M, De MR, D'Haene N, et al. Unspecific post-mortem findings despite multiorgan viral spread in COVID-19 patients. Crit Care 2020;24:495
39. Solomon IH, Normandin E, Bhattacharyya S, et al. Neuropathological features of Covid-19. N Engl J Med 2020;383:989–92
40. Lopez G, Tonello C, Osipova G, et al. Olfactory bulb SARS-CoV-2 infection is not paralleled by the presence of virus in other central nervous system areas. Neuropathol Appl Neurobiol 2022;48:e12752
41. Pilotto A, Odolini S, Masciocchi S, et al. Steroid-responsive encephalitis in Coronavirus Disease 2019. Ann Neurol 2020;88:423–7
42. Poyiadji N, Shahin G, Noujaim D, et al. COVID-19-associated acute hemorrhagic necrotizing encephalopathy: Imaging features. Radiology 2020;296:E119–20
43. Moriguchi T, Harii N, Goto J, et al. A first case of meningitis/encephalitis associated with SARS-Coronavirus-2. Int J Infect Dis 2020;94:55–8
44. Mao L, Jin H, Wang M, et al. Neurologic manifestations of hospitalized patients with Coronavirus Disease 2019 in Wuhan, China. JAMA Neurol 2020;77:683–90
45. von Weyhern CH, Kaufmann I, Neff F, et al. Early evidence of pronounced brain involvement in fatal COVID-19 outcomes. Lancet 2020; 395:e109
46. Al-Dalahmah O, Thakur KT, Nordvig AS, et al. Neuronophagia and microglial nodules in a SARS-CoV-2 patient with cerebellar hemorrhage. Acta Neuropathol Commun 2020;8:147
47. Bradley BT, Maioli H, Johnston R, et al. Histopathology and ultrastructural findings of fatal COVID-19 infections in Washington State: A case series. Lancet 2020;396:320–32
48. Bryce C, Grimes Z, Pujadas E, et al. Pathophysiology of SARS-CoV-2: The Mount Sinai COVID-19 autopsy experience. Mod Pathol 2021;34: 1456–67
49. Poisson KE, Zygmunt A, Fuller LD, et al. Lethal pediatric cerebral vasculitis triggered by severe acute respiratory syndrome Coronavirus 2. Pediatr Neurol 2022;127:1–5
50. Colombo D, Falasca L, Marchioni L, et al. Neuropathology and inflammatory cell characterization in 10 autoptic COVID-19 brains. Cells 2021;10:2262
51. Ludlow M, Kortekaas J, Herden C, et al. Neurotropic virus infections as the cause of immediate and delayed neuropathology. Acta Neuropathol 2016;131:159–84
52. Seilhean D. Infections of the central nervous system: Neuropathology. Rev Neurol (Paris) 2019;175:431–5
53. Conklin J, Frosch MP, Mukerji S, et al. Cerebral microvascular injury in severe COVID-19. medRxiv 2020;doi: 10.1101/2020.07.21.20159376
54. Jaunmuktane Z, Mahadeva U, Green A, et al. Microvascular injury and hypoxic damage: Emerging neuropathological signatures in COVID-19. Acta Neuropathol 2020;140:397–400
55. Reichard RR, Kashani KB, Boire NA, et al. Neuropathology of COVID-19: A spectrum of vascular and acute disseminated encephalomyelitis (ADEM)-like pathology. Acta Neuropathol 2020;140:1–6
56. Keller E, Brandi G, Winklhofer S, et al. Large and small cerebral vessel involvement in severe COVID-19: Detailed clinical workup of a case series. Stroke 2020;51:3719–22
57. Borczuk AC, Salvatore SP, Seshan SV, et al. COVID-19 pulmonary pathology: A multi-institutional autopsy cohort from Italy and New York City. Mod Pathol 2020;33:2156–68
58. Song E, Zhang C, Israelow B, et al. Neuroinvasion of SARS-CoV-2 in human and mouse brain. K Exp Med 2021;18:e20202135
59. Satturwar S, Fowkes M, Farver C, et al. Postmortem findings associated with SARS-CoV-2: Systematic review and meta-analysis. Am J Surg Pathol 2021;45:587–603
60. Schaller T, Hirschbuhl K, Burkhardt K, et al. Postmortem examination of patients with COVID-19. JAMA 2020;323:2518–20
61. Schurink B, Roos E, Radonic T, et al. Viral presence and immunopathology in patients with lethal COVID-19: A prospective autopsy cohort study. Lancet Microbe 2020;1:e290–9
62. Schwabenland M, Salie H, Tanevski J, et al. Deep spatial profiling of human COVID-19 brains reveals neuroinflammation with distinct microanatomical microglia-T-cell interactions. Immunity 2021;54: 1594–610
63. Lima M, Siokas V, Aloizou AM, et al. Unraveling the possible routes of SARS-COV-2 invasion into the central nervous system. Curr Treat Options Neurol 2020;22:37
64. Bhatta S, Sharma D, Sharma S, et al. Smell and taste disturbance in COVID-19 patients: A prospective multicenter review. Indian J Otolaryngol Head Neck Surg 2021;1–7. doi:10.1007/s12070-021-02664-z
65. Levinson R, Elbaz M, Ben-Ami R, et al. Time course of anosmia and dysgeusia in patients with mild SARS-CoV-2 infection. Infect Dis (Lond) 2020;52:600–2
66. Eliezer M, Hautefort C, Hamel AL, et al. Sudden and complete olfactory loss function as a possible symptom of COVID-19. JAMA Otolaryngol Head Neck Surg 2020;146:674–5
67. Cantuti-Castelvetri L, Ojha R, Pedro LD, et al. Neuropilin-1 facilitates SARS-CoV-2 cell entry and infectivity. Science 2020;370:856–60
68. Lapina C, Rodic M, Peschanski D, et al. The potential genetic network of human brain SARS-CoV-2 infection. Biorxiv 2020; doi: 10.1101/2020.04.06.027318
69. Kabbani N, Olds JL. Does COVID19 infect the brain? If so, smokers might be at a higher risk. Mol Pharmacol 2020;97:351–3
70. Butowt R, Bilinska K. SARS-CoV-2: Olfaction, brain infection, and the urgent need for clinical samples allowing earlier virus detection. ACS Chem Neurosci 2020;11:1200–3
71. Hawrylycz MJ, Lein ES, Guillozet-Bongaarts AL, et al. An anatomically comprehensive atlas of the adult human brain transcriptome. Nature 2012;489:391–9
72. Netland J, Meyerholz DK, Moore S, et al. Severe acute respiratory syndrome coronavirus infection causes neuronal death in the absence of encephalitis in mice transgenic for human ACE2. J Virol 2008;82: 7264–75
73. Mizgerd JP. Inflammation and pneumonia: Why are some more susceptible than others? Clin Chest Med 2018;39:669–76
74. Lipsitch M, Viboud C. Influenza seasonality: Lifting the fog. Proc Natl Acad Sci USA 2009;106:3645–6
75. Martinez ME. The calendar of epidemics: Seasonal cycles of infectious diseases. PLoS Pathog 2018;14:e1007327
76. Frasca D, McElhaney J. Influence of obesity on pneumococcus infection risk in the elderly. Front Endocrinol (Lausanne) 2019;10:71
77. Hespanhol V, Barbara C. Pneumonia mortality, do comorbidities matter? Pulmonology 2020;26:123–9
78. Kalil AC, Thomas PG. Influenza virus-related critical illness: Pathophysiology and epidemiology. Crit Care 2019;23:258
79. Peters SAE, MacMahon S, Woodward M. Obesity as a risk factor for COVID-19 mortality in women and men in the UK biobank: Comparisons with influenza/pneumonia and coronary heart disease. Diabetes Obes Metab 2021;23:258–62
80. Suleyman G, Fadel RA, Malette KM, et al. Clinical characteristics and morbidity associated with coronavirus disease 2019 in a Series of Patients in Metropolitan Detroit. JAMA Netw Open 2020;3: e2012270
81. Richardson S, Hirsch JS, Narasimhan M, et al.; the Northwell COVID-19 Research Consortium. Presenting characteristics, comorbidities, and outcomes among 5700 patients hospitalized with COVID-19 in the New York City area. JAMA 2020;323:2052–9
82. Engin AB, Engin ED, Engin A. Two important controversial risk factors in SARS-CoV-2 infection: Obesity and smoking. Environ Toxicol Pharmacol 2020;78:103411
83. Palaiodimos L, Kokkinidis DG, Li W, et al. Severe obesity, increasing age and male sex are independently associated with worse in-hospital outcomes, and higher in-hospital mortality, in a cohort of patients with COVID-19 in the Bronx, New York. Metabolism 2020;108:154262
84. Kaplan V, Angus DC, Griffin MF, et al. Hospitalized community-acquired pneumonia in the elderly: Age- and sex-related patterns of care and outcome in the United States. Am J Respir Crit Care Med 2002;165:766–72
85. Pasquale CB, Vietri J, Choate R, et al. Patient-reported consequences of community-acquired pneumonia in patients with chronic obstructive pulmonary disease. Chronic Obstr Pulm Dis 2019;6:132–44
86. Patil A, Tripathy JP, Deshmukh V, et al. Sex hormones and COVID-19: Tussle between the two. Monaldi Arch Chest Dis 2020;90. doi: 10.4081/monaldi.2020.1461
87. Aggarwal G, Lippi G, Lavie CJ, et al. Diabetes mellitus association with coronavirus disease 2019 (COVID-19) severity and mortality: A pooled analysis. J Diabetes 2020;12:851–5
88. Aggarwal G, Lippi G, Michael HB. Cerebrovascular disease is associated with an increased disease severity in patients with Coronavirus

Disease 2019 (COVID-19): A pooled analysis of published literature. Int J Stroke 2020;15:385–9
89. Aggarwal G, Cheruiyot I, Aggarwal S, et al. Association of cardiovascular disease with Coronavirus Disease 2019 (COVID-19) severity: A meta-analysis. Curr Probl Cardiol 2020;45:100617
90. Edler C, Schroder AS, Aepfelbacher M, et al. Dying with SARS-CoV-2 infection-an autopsy study of the first consecutive 80 cases in Hamburg, Germany. Int J Legal Med 2020;134:1275–84
91. Gebhard C, Regitz-Zagrosek V, Neuhauser HK, et al. Impact of sex and gender on COVID-19 outcomes in Europe. Biol Sex Differ 2020; 11:29
92. Ssentongo P, Ssentongo AE, Heilbrunn ES, et al. Association of cardiovascular disease and 10 other pre-existing comorbidities with COVID-19 mortality: A systematic review and meta-analysis. PLoS One 2020; 15:e0238215
93. Hussain A, Mahawar K, Xia Z, et al. Obesity and mortality of COVID-19. Meta-analysis. Obes Res Clin Pract 2020;14:295–300
94. Attems J, Konig C, Huber M, et al. Cause of death in demented and non-demented elderly inpatients; an autopsy study of 308 cases. J Alzheimers Dis 2005;8:57–62
95. Wang X, You G, Chen H, et al. Clinical course and cause of death in elderly patients with idiopathic Parkinson's disease. Chin Med J (Engl) 2002;115:1409–11
96. Degerskar ANW, Englund EM. Cause of death in autopsy-confirmed dementia disorders. Eur J Neurol 2020;27:2415–21
97. Litvan I, Mangone CA, McKee A, et al. Natural history of progressive supranuclear palsy (Steele-Richardson-Olszewski syndrome) and clinical predictors of survival: A clinicopathological study. J Neurol Neurosurg Psychiatry 1996;60:615–20
98. Shea YF, Shum ACK, Lee SC, et al. Natural clinical course of progressive supranuclear palsy in Chinese patients in Hong Kong. Hong Kong Med J 2019;25:444–52
99. Covino M, De MG, Santoro M, et al. Clinical characteristics and prognostic factors in COVID-19 patients aged >/=80 years. Geriatr Gerontol Int 2020;20:704–8
100. Atkins JL, Masoli JAH, Delgado J, et al. Preexisting comorbidities predicting COVID-19 and mortality in the UK Biobank community cohort. J Gerontol A Biol Sci Med Sci 2020;75:2224–30
101. Beatty JA, Majumdar SR, Tyrrell GJ, et al. Prognostic factors associated with mortality and major in-hospital complications in patients with bacteremic pneumococcal pneumonia: Population-based study. Medicine (Baltimore) 2016;95:e5179
102. Noguchi S, Yatera K, Kato T, et al. Impact of the number of aspiration risk factors on mortality and recurrence in community-onset pneumonia. Clin Interv Aging 2017;12:2087–94
103. Rao A, Suliman A, Vuik S, et al. Outcomes of dementia: Systematic review and meta-analysis of hospital administrative database studies. Arch Gerontol Geriatr 2016;66:198–204
104. Boivin Z, Perez MF, Atuegwu NC, et al. Association of atypical antipsychotics and mortality for patients hospitalised with pneumonia. ERJ Open Res 2019;5:00223–2018
105. Fall PA, Saleh A, Fredrickson M, et al. Survival time, mortality, and cause of death in elderly patients with Parkinson's disease: A 9-year follow-up. Mov Disord 2003;18:1312–6
106. Magaki S, Yong WH, Khanlou N, et al. Comorbidity in dementia: Update of an ongoing autopsy study. J Am Geriatr Soc 2014;62:1722–8
107. Foley NC, Affoo RH, Martin RE. A systematic review and meta-analysis examining pneumonia-associated mortality in dementia. Dement Geriatr Cogn Disord 2015;39:52–67
108. Manabe T, Mizukami K, Akatsu H, et al. Prognostic factors related to dementia with Lewy bodies complicated with pneumonia: An autopsy study. Intern Med 2016;55:2771–6
109. Chang YP, Yang CJ, Hu KF, et al. Risk factors for pneumonia among patients with Parkinson's disease: A Taiwan nationwide population-based study. Neuropsychiatr Dis Treat 2016;12:1037–46
110. Nath U, Thomson R, Wood R, et al. Population based mortality and quality of death certification in progressive supranuclear palsy (Steele-Richardson-Olszewski syndrome). J Neurol Neurosurg Psychiatry 2005;76:498–502
111. Manabe T, Fujikura Y, Mizukami K, et al. Pneumonia-associated death in patients with dementia: A systematic review and meta-analysis. PLoS One 2019;14:e0213825
112. Beach TG, Russell A, Sue LI, et al. Increased risk of autopsy-proven pneumonia with sex, season and neurodegenerative disease. medRxiv 2021;doi:10.1101/2021.01.07.21249410
113. Kurki SN, Kantonen J, Kaivola K, et al.; FinnGen. APOE epsilon4 associates with increased risk of severe COVID-19, cerebral microhaemorrhages and post-COVID mental fatigue: A Finnish biobank, autopsy and clinical study. Acta Neuropathol Commun 2021;9:199
114. Lee WE, Park SW, Weinberger DM, et al. Direct and indirect mortality impacts of the COVID-19 pandemic in the US, March 2020-April 2021. medRxiv 2022;doi:10.1101/2022.02.10.22270721
115. Kuo CL, Pilling LC, Atkins JL, et al. ApoE e4e4 genotype and mortality with COVID-19 in UK Biobank. J Gerontol A Biol Sci Med Sci 2020; 75:1801–3
116. Kuo CL, Pilling LC, Atkins JL, et al. APOE e4 genotypes increase risk of delirium during COVID-19-related hospitalizations: Evidence from a large UK cohort. J Gerontol A Biol Sci Med Sci 2022;77:879–80
117. Kasparian K, Graykowski D, Cudaback E. Commentary: APOE e4 genotype predicts severe COVID-19 in the UK Biobank Community Cohort. Front Immunol 2020;11:1939
118. Kuo CL, Melzer D. Response to comment on "ApoE e4e4 genotype and mortality with COVID-19 in UK Biobank" by Kuo, et al. J Gerontol A Biol Sci Med Sci 2020;75:2235–6
119. Nikogosov DA, Shevlyakov AD, Baranova AV. Comment on "ApoE e4e4 genotype and mortality with COVID-19 in UK Biobank" by Kuo, et al. J Gerontol A Biol Sci Med Sci 2020;75:2233–4
120. Mann DM, Yates PO, Davies JS, et al. Viruses, parkinsonism and Alzheimer's disease. J Neurol Neurosurg Psychiatry 1981;44:651
121. Jamieson GA, Maitland NJ, Wilcock GK, et al. Latent herpes simplex virus type 1 in normal and Alzheimer's disease brains. J Med Virol 1991;33:224–7
122. Sequiera LW, Jennings LC, Carrasco LH, et al. Detection of herpes-simplex viral genome in brain tissue. Lancet 1979;2:609–12
123. Fraser NW, Lawrence WC, Wroblewska Z, et al. Herpes simplex type 1 DNA in human brain tissue. Proc Natl Acad Sci USA 1981;78:6461–5
124. Roberts GW, Taylor GR, Carter GI, et al. Herpes simplex virus: A role in the aetiology of Alzheimer's disease? J Neurol Neurosurg Psychiatry 1986;49:216
125. Itzhaki RF, Golde TE, Heneka MT, et al. Do infections have a role in the pathogenesis of Alzheimer disease? Nat Rev Neurol 2020;16:193–7
126. Gamboa ET, Wolf A, Yahr MD, et al. Influenza virus antigen in postencephalitic parkinsonism brain. Detection by immunofluorescence. Arch Neurol 1974;31:228–32
127. Beach TG, Adler CH, Sue LI, et al. Arizona study of aging and neurodegenerative disorders and brain and body donation program. Neuropathology 2015;35:354–89
128. Nelson PT, Dickson DW, Trojanowski JQ, et al. Limbic-predominant age-related TDP-43 encephalopathy (LATE): Consensus working group report. Brain 2019;142:1503–27
129. Dickson DW, Rademakers R, Hutton ML. Progressive supranuclear palsy: Pathology and genetics. Brain Pathol 2007;17:74–82
130. Dickson DW, Ahmed Z, Algom AA, et al. Neuropathology of variants of progressive supranuclear palsy. Curr Opin Neurol 2010;23:394–400
131. Crary JF, Trojanowski JQ, Schneider JA, et al. Primary age-related tauopathy (PART): A common pathology associated with human aging. Acta Neuropathol 2014;128:755–66
132. Kovacs GG, Ferrer I, Grinberg LT, et al. Aging-related tau astrogliopathy (ARTAG): Harmonized evaluation strategy. Acta Neuropathol 2016;131:87–102
133. Roman GC, Tatemichi TK, Erkinjuntti T, et al. Vascular dementia: Diagnostic criteria for research studies. Report of the NINDS-AIREN International Workshop. Neurology 1993;43:250–60
134. Mackenzie IR, Neumann M, Baborie A, et al. A harmonized classification system for FTLD-TDP pathology. Acta Neuropathol 2011;122: 111–3
135. Gelb DJ, Oliver E, Gilman S. Diagnostic criteria for Parkinson disease. Arch Neurol 1999;56:33–9
136. Dickson DW, Braak H, Duda JE, et al. Neuropathological assessment of Parkinson's disease: Refining the diagnostic criteria. Lancet Neurol 2009;8:1150–7
137. Dickson DW. Required techniques and useful molecular markers in the neuropathologic diagnosis of neurodegenerative diseases. Acta Neuropathol 2005;109:14–24

138. Hyman BT, Phelps CH, Beach TG, et al. National Institute on Aging-Alzheimer's Association guidelines for the neuropathologic assessment of Alzheimer's disease. Alzheimers Dement 2012;8:1–13
139. Montine TJ, Phelps CH, Beach TG, et al.; Alzheimer's Association. National Institute on Aging-Alzheimer's Association guidelines for the neuropathologic assessment of Alzheimer's disease: A practical approach. Acta Neuropathol 2012;123:1–11
140. McKeith IG, Dickson DW, Lowe J, et al.; Consortium on DLB. Diagnosis and management of dementia with Lewy bodies: Third report of the DLB Consortium. Neurology 2005;65:1863–72
141. Tremblay C, Beach TG, Intorcia AJ, et al. Deafferentation of olfactory bulb in subjects dying with COVID-19. medRxiv 2021;doi: 10.1101/2021.12.21.21268119
142. Baba Y, Ghetti B, Baker MC, et al. Hereditary diffuse leukoencephalopathy with spheroids: Clinical, pathologic and genetic studies of a new kindred. Acta Neuropathol 2006;111:300–11
143. Corman VM, Landt O, Kaiser M, et al. Detection of 2019 novel coronavirus (2019-nCoV) by real-time RT-PCR. Euro Surveill 2020;25: 2000045
144. Zhen W, Berry GJ. Development of a new multiplex real-time RT-PCR assay for severe acute respiratory syndrome coronavirus 2 (SARS-CoV-2) detection. J Mol Diagn 2020;22:1367–72
145. Dobin A, Davis CA, Schlesinger F, et al. STAR: Ultrafast universal RNA-seq aligner. Bioinformatics 2013;29:15–21
146. Ewels P, Magnusson M, Lundin S, et al. MultiQC: Summarize analysis results for multiple tools and samples in a single report. Bioinformatics 2016;32:3047–8
147. Mathys H, Davila-Velderrain J, Peng Z, et al. Single-cell transcriptomic analysis of Alzheimer's disease. Nature 2019;570:332–7
148. Satija R, Farrell JA, Gennert D, et al. Spatial reconstruction of single-cell gene expression data. Nat Biotechnol 2015;33:495–502
149. Langfelder P, Horvath S. WGCNA: An R package for weighted correlation network analysis. BMC Bioinformatics 2008;9:559
150. Law CW, Chen Y, Shi W, et al. voom: Precision weights unlock linear model analysis tools for RNA-seq read counts. Genome Biol 2014;15: R29
151. Ritchie ME, Phipson B, Wu D, et al. limma powers differential expression analyses for RNA-sequencing and microarray studies. Nucleic Acids Res 2015;43:e47
152. Zhang B, Horvath S. A general framework for weighted gene co-expression network analysis. Stat Appl Genet Mol Biol 2005;4: Article17
153. Langfelder P, Horvath S. Eigengene networks for studying the relationships between co-expression modules. BMC Syst Biol 2007;1:54
154. Serrano GE, Walker JE, Arce R, et al. Mapping of SARS-CoV-2 brain invasion and histopathology in COVID-19 disease. medRxiv 2021;doi: 10.1101/2021.02.15.21251511
155. Piras IS, Huentelman J, Walker JE, et al. Olfactory bulb and amygdala gene expression changes in subjects dying with COVID-19. medRxiv 2021;doi:10.1101/2021.09.12.21263291
156. Beach TG, DeTure M, Walker JE, et al. White matter β-amyloid precursor protein immunoreactivity in autopsied subjects with and without COVID-19. medRxiv 2021;doi:10.1101/2021.12.16.21266656
157. Wolfel R, Corman VM, Guggemos W, et al. Virological assessment of hospitalized patients with COVID-2019. Nature 2020;581:465–9
158. Park C, Lee J, Hassan ZU, et al. Comparison of digital PCR and quantitative PCR with various SARS-CoV-2 primer-probe sets. J Microbiol Biotechnol 2021;31:358–67
159. Hur KH, Park K, Lim Y, et al. Evaluation of four commercial kits for SARS-CoV-2 real-time reverse-transcription polymerase chain reaction approved by emergency-use-authorization in Korea. Front Med (Lausanne) 2020;7:521
160. Hong KH, In JW, Lee J, et al. Prevalence of a single-nucleotide variant of SARS-CoV-2 in Korea and Its impact on the diagnostic sensitivity of the Xpert Xpress SARS-CoV-2 assay. Ann Lab Med 2022; 42:389
161. Barra GB, Santa Rita TH, Mesquita PG, et al. Analytical sensitivity and specificity of two RT-qPCR protocols for SARS-CoV-2 detection performed in an automated workflow. Genes (Basel) 2020;11:1183
162. Beach TG, Sue LI, Intorcia AJ, et al. Acute brain ischemia, infarction and hemorrhage in subjects dying with or without autopsy-proven acute pneumonia. medRxiv 2021;doi:10.1101/2021.03.22.21254139
163. Kirschenbaum D, Imbach LL, Rushing EJ, et al. Intracerebral endotheliitis and microbleeds are neuropathological features of COVID-19. Neuropathol Appl Neurobiol 2020;47:554–9
164. Piroth L, Cottenet J, Mariet AS, et al. Comparison of the characteristics, morbidity, and mortality of COVID-19 and seasonal influenza: A nationwide, population-based retrospective cohort study. Lancet Respir Med 2021;9:251–9
165. Nannoni S, de GR, Bell S, et al. Stroke in COVID-19: A systematic review and meta-analysis. Int J Stroke 2021;16:137–49
166. Coolen T, Lolli V, Sadeghi N, et al. Early postmortem brain MRI findings in COVID-19 non-survivors. Neurology 2020;95:e2016–27
167. Radmanesh A, Raz E, Zan E, et al. Brain imaging use and findings in COVID-19: A single academic center experience in the epicenter of disease in the United States. AJNR Am J Neuroradiol 2020;41:1179–83
168. Beyrouti R, Best JG, Chandratheva A, et al. Characteristics of intracerebral haemorrhage associated with COVID-19: A systematic review and pooled analysis of individual patient and aggregate data. J Neurol 2021; 268:3105–15
169. Beyrouti R, Adams ME, Benjamin L, et al. Characteristics of ischaemic stroke associated with COVID-19. J Neurol Neurosurg Psychiatry 2020;91:889–91
170. Diener HC, Berlit P, Masjuan J. COVID-19: Patients with stroke or risk of stroke. Eur Heart J Suppl 2020;22:25–8
171. Merkler AE, Parikh NS, Mir S, et al. Risk of ischemic stroke in patients with Coronavirus Disease 2019 (COVID-19) vs patients with influenza. JAMA Neurol 2020;77:1366–7
172. Nersesjan V, Amiri M, Christensen HK, et al. Thirty-day mortality and morbidity in COVID-19 positive vs. COVID-19 negative individuals and vs. individuals tested for Influenza A/B: A population-based study. Front Med (Lausanne) 2020;7:598272
173. Ramos-Araque ME, Siegler JE, Ribo M, et al.; SVIN Multinational Registry and Task Force. Stroke etiologies in patients with COVID-19: The SVIN COVID-19 multinational registry. BMC Neurol 2021;21:43
174. Rothstein A, Oldridge O, Schwennesen H, et al. Acute cerebrovascular events in hospitalized COVID-19 patients. Stroke 2020;51:e219–22
175. Siow I, Lee KS, Zhang JJY, et al. Stroke as a neurological complication of COVID-19: A systematic review and meta-analysis of incidence, outcomes and predictors. J Stroke Cerebrovasc Dis 2021;30:105549
176. Allegra A, Innao V, Allegra AG, et al. Coagulopathy and thromboembolic events in patients with SARS-CoV-2 infection: Pathogenesis and management strategies. Ann Hematol 2020;99:1953–65
177. McFadyen JD, Stevens H, Peter K. The emerging threat of (micro)thrombosis in COVID-19 and its therapeutic implications. Circ Res 2020;127:571–87
178. Crunfli F, Carregari VC, Veras FP, et al. Morphological, cellular and molecular basis of brain infection in COVID-19 patients. medRxiv 2022;doi:10.1101/2020.10.09.20207464
179. Amruta N, Chastain WH, Paz M, et al. SARS-CoV-2 mediated neuroinflammation and the impact of COVID-19 in neurological disorders. Cytokine Growth Factor Rev 2021;58:1–15
180. Yang AC, Kern F, Losada PM, et al. Dysregulation of brain and choroid plexus cell types in severe COVID-19. Nature 2021;595:565–71
181. Iwata H, Goettsch C, Sharma A, et al. PARP9 and PARP14 cross-regulate macrophage activation via STAT1 ADP-ribosylation. Nat Commun 2016;7:12849
182. Zhang Y, Mao D, Roswit WT, et al. PARP9-DTX3L ubiquitin ligase targets host histone H2BJ and viral 3C protease to enhance interferon signaling and control viral infection. Nat Immunol 2015;16:1215–27
183. Russo LC, Tomasin R, Matos IA, et al. The SARS-CoV-2 Nsp3 macrodomain reverses PARP9/DTX3L-dependent ADP-ribosylation induced by interferon signaling. J Biol Chem 2021;297:101041
184. Tahamtan A, Tavakoli-Yaraki M, Rygiel TP, et al. Effects of cannabinoids and their receptors on viral infections. J Med Virol 2016;88:1–12
185. Nicole O, Pacary E. CaMKIIbeta in neuronal development and plasticity: An emerging candidate in brain diseases. IJMS 2020;21:7272
186. Kury S, van Woerden GM, Besnard T, et al.; Deciphering Developmental Disorders Study. De novo mutations in protein kinase genes CAMK2A and CAMK2B cause intellectual disability. Am J Hum Genet 2017;101:768–88
187. Akita T, Aoto K, Kato M, et al. De novo variants in CAMK2A and CAMK2B cause neurodevelopmental disorders. Ann Clin Transl Neurol 2018;5:280–96

188. Rizzi S, Spagnoli C, Salerno GG, et al. Severe intellectual disability, absence of language, epilepsy, microcephaly and progressive cerebellar atrophy related to the recurrent de novo variant p.(P139L) of the CAMK2B gene: A case report and brief review. Am J Med Genet A 2020;182:2675–9
189. Woo MS, Malsy J, Pottgen J, et al. Frequent neurocognitive deficits after recovery from mild COVID-19. Brain Commun 2020;2:fcaa205
190. Vasek MJ, Garber C, Dorsey D, et al. A complement-microglial axis drives synapse loss during virus-induced memory impairment. Nature 2016;534:538–43
191. Daniels BP, Holman DW, Cruz-Orengo L, et al. Viral pathogen-associated molecular patterns regulate blood-brain barrier integrity via competing innate cytokine signals. mBio 2014;5:e01476–14
192. Liddelow SA, Guttenplan KA, Clarke LE, et al. Neurotoxic reactive astrocytes are induced by activated microglia. Nature 2017;541:481–7
193. Twardowski T, Fertala A, Orgel JP, et al. Type I collagen and collagen mimetics as angiogenesis promoting superpolymers. Curr Pharm Des 2007;13:3608–21
194. Ostergaard L. SARS CoV-2 related microvascular damage and symptoms during and after COVID-19: Consequences of capillary transit-time changes, tissue hypoxia and inflammation. Physiol Rep 2021;9: e14726
195. Ackermann M, Mentzer SJ, Kolb M, et al. Inflammation and intussusceptive angiogenesis in COVID-19: Everything in and out of flow. Eur Respir J 2020;56:2003147
196. Jiao L, Yang Y, Yu W, et al. The olfactory route is a potential way for SARS-CoV-2 to invade the central nervous system of rhesus monkeys. Signal Transduct Target Ther 2021;6:169
197. Ye Q, Zhou J, He Q, et al. SARS-CoV-2 infection in the mouse olfactory system. Cell Discov 2021;7:49
198. Monchatre-Leroy E, Lesellier S, Wasniewski M, et al. Hamster and ferret experimental infection with intranasal low dose of a single strain of SARS-CoV-2. J Gen Virol 2021;102:001567
199. de Melo GD, Lazarini F, Levallois S, et al. COVID-19-related anosmia is associated with viral persistence and inflammation in human olfactory epithelium and brain infection in hamsters. Sci Transl Med 2021; 13:eabf8396
200. Zhang AJ, Lee AC, Chu H, et al. Severe acute respiratory syndrome coronavirus 2 infects and damages the mature and immature olfactory sensory neurons of hamsters. Clin Infect Dis 2021;73:e503–12
201. Margolis FL. Olfactory marker protein (OMP). Scand J Immunol Suppl 1982;9:181–99
202. Monti-Graziadei GA, Margolis FL, Harding JW, et al. Immunocytochemistry of the olfactory marker protein. J Histochem Cytochem 1977; 25:1311–6
203. Wensley CH, Stone DM, Baker H, et al. Olfactory marker protein mRNA is found in axons of olfactory receptor neurons. J Neurosci 1995;15:4827–37
204. Biffo S, DeLucia R, Mulatero B, et al. Carnosine-, calcitonin gene-related peptide- and tyrosine hydroxylase-immunoreactivity in the mouse olfactory bulb following peripheral denervation. Brain Res 1990;528:353–7
205. Byrd CA. Deafferentation-induced changes in the olfactory bulb of adult zebrafish. Brain Res 2000;866:92–100
206. Cummings DM, Emge DK, Small SL, et al. Pattern of olfactory bulb innervation returns after recovery from reversible peripheral deafferentation. J Comp Neurol 2000;421:362–73
207. Verhaagen J, Oestreicher AB, Grillo M, et al. Neuroplasticity in the olfactory system: Differential effects of central and peripheral lesions of the primary olfactory pathway on the expression of B-50/GAP43 and the olfactory marker protein. J Neurosci Res 1990;26:31–44
208. Buiakova OI, Baker H, Scott JW, et al. Olfactory marker protein (OMP) gene deletion causes altered physiological activity of olfactory sensory neurons. Proc Natl Acad Sci USA 1996;93:9858–63
209. Lorenzon P, Redolfi N, Podolsky MJ, et al. Circuit formation and function in the olfactory bulb of mice with reduced spontaneous afferent activity. J Neurosci 2015;35:146–60
210. Redolfi N, Lodovichi C. Spontaneous afferent activity carves olfactory circuits. Front Cell Neurosci 2021;15:637536
211. Kikusui T, Kajita M, Otsuka N, et al. Sex differences in olfactory-induced neural activation of the amygdala. Behav Brain Res 2018;346: 96–104
212. Kim HH, Puche AC, Margolis FL. Odorant deprivation reversibly modulates transsynaptic changes in the NR2B-mediated CREB pathway in mouse piriform cortex. J Neurosci 2006;26:9548–59
213. Koliatsos VE, Dawson TM, Kecojevic A, et al. Cortical interneurons become activated by deafferentation and instruct the apoptosis of pyramidal neurons. Proc Natl Acad Sci USA 2004;101:14264–9
214. Capurso SA, Calhoun ME, Sukhov RR, et al. Deafferentation causes apoptosis in cortical sensory neurons in the adult rat. J Neurosci 1997;17: 7372–84
215. Zhou L, Welsh AM, Chen D, et al. NMDA inhibitors cause apoptosis of pyramidal neurons in mature piriform cortex: Evidence for a nitric oxide-mediated effect involving inhibitory interneurons. Neuropharmacology 2007;52:1528–37
216. Leung CH, Wilson DA. Trans-neuronal regulation of cortical apoptosis in the adult rat olfactory system. Brain Res 2003;984:182–8
217. Ammar A, Distinguin L, Chetrit A, et al. Transient modifications of the olfactory bulb on MR follow-up of COVID-19 patients with related olfactory dysfunction. J Neuroradiol 2022;49:329–32
218. Altunisik E, Baykan AH, Sahin S, et al. Quantitative analysis of the olfactory system in COVID-19: An MR Imaging study. AJNR Am J Neuroradiol 2021;42:2207–14
219. Douaud G, Lee S, Alfaro-Almagro F, et al. SARS-CoV-2 is associated with changes in brain structure in UK Biobank. Nature 2022;604: 697–707
220. Guedj E, Campion JY, Dudouet P, et al. (18)F-FDG brain PET hypometabolism in patients with long COVID. Eur J Nucl Med Mol Imaging 2021;48:2823–33
221. Skeli I, Sato H, Diksic M. Olfactory bulbectomy reduces cerebral glucose utilization: 2-[14C]deoxyglucose autoradiographic study. Brain Res Bull 2008;76:485–92
222. Khan M, Yoo SJ, Clijsters M, et al. Visualizing in deceased COVID-19 patients how SARS-CoV-2 attacks the respiratory and olfactory mucosae but spares the olfactory bulb. Cell 2021;184:5932–49
223. Kelly JP, Wrynn AS, Leonard BE. The olfactory bulbectomized rat as a model of depression: An update. Pharmacol Ther 1997;74: 299–316
224. Leonard BE. The olfactory bulbectomized rat as a model of depression. Pol J Pharmacol Pharm 1984;36:561–9
225. Skelin I, Kovacevic T, Sato H, et al. Upregulated arachidonic acid signalling in the olfactory bulbectomized rat model of depression. Neurochem Int 2011;58:483–8
226. Wrynn AS, Sebens JB, Koch T, et al. Prolonged c-Jun expression in the basolateral amygdala following bulbectomy: Possible implications for antidepressant activity and time of onset. Brain Res Mol Brain Res 2000;76:7–17
227. Burke NN, Geoghegan E, Ker DM, et al. Altered neuropathic pain behaviour in a rat model of depression is associated with changes in inflammatory gene expression in the amygdala. Genes Brain Behav 2013; 12:705–13
228. Takahashi K, Tsuji M, Nakagawasai O, et al. Activation of cholinergic system partially rescues olfactory dysfunction-induced learning and memory deficit in mice. Behav Brain Res 2021;408:113283
229. Moriguchi S, Inagaki R, Fukunaga K. Memantine improves cognitive deficits via KATP channel inhibition in olfactory bulbectomized mice. Mol Cell Neurosci 2021;117:103680
230. Moriguchi S, Inagaki R, Shimojo H, et al. Memantine improves depressive-like behaviors via Kir6.1 channel inhibition in olfactory bulbectomized mice. Neuroscience 2020;442:264–73
231. Yabuki Y, Matsuo K, Hirano K, et al. Combined memantine and donepezil treatment improves behavioral and psychological symptoms of dementia-like behaviors in olfactory bulbectomized mice. Pharmacology 2017;99:160–71
232. Bobkova N, Vorobyov V, Medvinskaya N, et al. Immunization against specific fragments of neurotrophin p75 receptor protects forebrain cholinergic neurons in the olfactory bulbectomized mice. J Alzheimers Dis 2016;53:289–301
233. D'Alessio FR, Heller NM. COVID-19 and myeloid cells: Complex interplay correlates with lung severity. J Clin Invest 2020;130: 6214–7
234. Manunta MDI, Lamorte G, Ferrari F, et al. Impact of SARS-CoV-2 infection on the recovery of peripheral blood mononuclear cells by density gradient. Sci Rep 2021;11:4904

235. Remy KE, Mazer M, Striker DA, et al. Severe immunosuppression and not a cytokine storm characterizes COVID-19 infections. JCI Insight 2020;5:e140329
236. Zingaropoli MA, Nijhawan P, Carraro A, et al. Increased sCD163 and sCD14 plasmatic levels and depletion of peripheral blood pro-inflammatory monocytes, myeloid and plasmacytoid dendritic cells in patients with severe COVID-19 pneumonia. Front Immunol 2021;12:627548
237. Haslbauer JD, Matter MS, Stalder AK, et al. Histomorphological patterns of regional lymph nodes in COVID-19 lungs. Pathologe 2021;42:89–97
238. Kaneko N, Kuo HH, Boucau J, et al.; Massachusetts Consortium on Pathogen Readiness Specimen Working Group. Loss of Bcl-6-expressing T follicular helper cells and germinal centers in COVID-19. Cell 2020;183:143–57
239. Röltgen K, Nielsen SCA, Silva O, et al. Immune imprinting, breadth of variant recognition, and germinal center response in human SARS-CoV-2 infection and vaccination. Cell 2022;185:1025–40
240. Liu C, Martins AJ, Lau WW, et al.; COVID Clinicians. Time-resolved systems immunology reveals a late juncture linked to fatal COVID-19. Cell 2021;184:1836–57
241. Bachstetter AD, Van Eldik LJ, Schmitt FA, et al. Disease-related microglia heterogeneity in the hippocampus of Alzheimer's disease, dementia with Lewy bodies, and hippocampal sclerosis of aging. Acta Neuropathol Commun 2015;3:32
242. Martini AC, Helman AM, McCarty KL, et al. Distribution of microglial phenotypes as a function of age and Alzheimer's disease neuropathology in the brains of people with Down syndrome. Alzheimers Dement (Amst) 2020;12:e12113
243. Shahidehpour RK, Higdon RE, Crawford NG, et al. Dystrophic microglia are associated with neurodegenerative disease and not healthy aging in the human brain. Neurobiol Aging 2021;99:19–27
244. Swanson MEV, Murray HC, Ryan B, et al. Quantitative immunohistochemical analysis of myeloid cell marker expression in human cortex captures microglia heterogeneity with anatomical context. Sci Rep 2020;10:11693
245. Streit WJ, Xue QS, Tischer J, et al. Microglial pathology. Acta Neuropathol Commun 2014;2:142
246. Loftus TJ, Ungaro R, Dirain M, et al. Overlapping but disparate inflammatory and Immunosuppressive responses to SARS-CoV-2 and bacterial sepsis: An immunological time course analysis. Front Immuno 2021;12:792448
247. Lucas C, Wong P, Klein J, et al.; Yale IMPACT Team. Longitudinal analyses reveal immunological misfiring in severe COVID-19. Nature 2020;584:463–9
248. Luporini RL, Rodolpho JMA, Kubota LT, et al. IL-6 and IL-10 are associated with disease severity and higher comorbidity in adults with COVID-19. Cytokine 2021;143:155507
249. Boldrini M, Canoll PD, Klein RS. How COVID-19 affects the brain. JAMA Psychiatry 2021;78:682–3
250. Turner GD, Bunthi C, Wonodi CB, et al. The role of postmortem studies in pneumonia etiology research. Clin Infect Dis 2012;54(Suppl 2): S165–71
251. Jain S, Self WH, Wunderink RG, et al.; CDC EPIC Study Team. Community-acquired pneumonia requiring hospitalization among U.S. Adults. N Engl J Med 2015;373:415–27
252. Morens DM, Taubenberger JK, Fauci AS. Predominant role of bacterial pneumonia as a cause of death in pandemic influenza: Implications for pandemic influenza preparedness. J Infect Dis 2008;198:962–70
253. Jang H, Boltz DA, Webster RG, et al. Viral parkinsonism. Biochim Biophys Acta 2009;1792:714–21
254. Allnutt MA, Johnson K, Bennett DA, et al. Human herpesvirus 6 detection in Alzheimer's disease cases and controls across multiple cohorts. Neuron 2020;105:1027–35
255. Desforges M, Le Coupanec A, Dubeau P, et al. Human coronaviruses and other respiratory viruses: Underestimated opportunistic pathogens of the central nervous system? Viruses 2019;12:14
256. Arbour N, Day R, Newcombe J, et al. Neuroinvasion by human respiratory coronaviruses. J Virol 2000;74:8913–21